IWMI Research Report

170

Mapping Multiple Climate-related Hazards in South Asia

Giriraj Amarnath, Niranga Alahacoon, Vladimir Smakhtin and Pramod Aggarwal

IWMI International Water Management Institute

UNITED NATIONS UNIVERSITY
UNU-INWEH
Institute for Water, Environment and Health

CGIAR
RESEARCH PROGRAM ON Climate Change, Agriculture and Food Security
CCAFS

Research Reports

The publications in this series cover a wide range of subjects—from computer modeling to experience with water user associations—and vary in content from directly applicable research to more basic studies, on which applied work ultimately depends. Some research reports are narrowly focused, analytical and detailed empirical studies; others are wide-ranging and synthetic overviews of generic problems.

Although most of the reports are published by IWMI staff and their collaborators, we welcome contributions from others. Each report is reviewed internally by IWMI staff, and by external reviewers. The reports are published and distributed both in hard copy and electronically (www.iwmi.org) and where possible all data and analyses will be available as separate downloadable files. Reports may be copied freely and cited with due acknowledgment.

About IWMI

IWMI's mission is to *provide evidence-based solutions to sustainably manage water and land resources for food security, people's livelihoods and the environment.* IWMI works in partnership with governments, civil society and the private sector to develop scalable agricultural water management solutions that have a tangible impact on poverty reduction, food security and ecosystem health.

IWMI Research Report 170

Mapping Multiple Climate-related Hazards in South Asia

Giriraj Amarnath, Niranga Alahacoon, Vladimir Smakhtin and Pramod Aggarwal

International Water Management Institute (IWMI)
P O Box 2075, Colombo, Sri Lanka

The authors: Giriraj Amarnath is Sub-Theme Leader: Water-related Disaster Risk Management at the headquarters of the International Water Management Institute (IWMI), Colombo, Sri Lanka; Niranga Alahacoon is RS/GIS Analyst at IWMI, Colombo, Sri Lanka; Vladimir Smakhtin is Director, United Nations University - Institute for Water, Environment and Health (UNU-INWEH), Ontario, Canada; and Pramod Aggarwal is Regional Program Leader at the CGIAR Research Program on Climate Change, Agriculture and Food Security (CCAFS) hosted by Borlaug Institute for South Asia (BISA), International Maize and Wheat Improvement Center (CIMMYT), New Delhi, India.

Amarnath, G.; Alahacoon, N.; Smakhtin, V.; Aggarwal, P. 2017. *Mapping multiple climate-related hazards in South Asia.* Colombo, Sri Lanka: International Water Management Institute (IWMI). 41p. (IWMI Research Report 170). doi: 10.5337/2017.207

/ climate change adaptation / natural disasters / weather hazards / mapping / flooding / drought / rain / erosion / temperature / sea level / water levels / coastal area / sloping land / tsunamis / agriculture / impact assessment / population / risk management / socioeconomic environment / land cover / South Asia / India / Bangladesh / Sri Lanka / Pakistan / Nepal /

ISSN 1026-0862
ISBN 978-92-9090-853-1

Front cover: Impact of floods and drought on people and agriculture (*all photos:* V. Dakshina Murthy/ IWMI).

Please send inquiries and comments to: IWMI-Publications@cgiar.org

A free copy of this publication can be downloaded at
www.iwmi.org/Publications/IWMI_Research_Reports/index.aspx

Acknowledgements

The authors would like to thank the National Aeronautics and Space Administration (NASA) for providing the Moderate Resolution Imaging Spectroradiometer (MODIS) datasets; Center for International Earth Science Information Network (CIESIN), Columbia University, Palisades, New York, USA, for providing the gridded population datasets; and Permanent Service for Mean Sea Level (PSMSL), National Oceanography Centre, UK, for providing sea-level data; and United States Geological Survey (USGS) for providing Landsat data. The assistance provided by Mr. Surajit Ghosh, Indian Institute of Remote Sensing (IIRS), India, with geographic information system (GIS) analysis is also gratefully acknowledged.

Collaborators

This research study is a collaboration of the following:

International Water Management Institute (IWMI)

United Nations University – Institute for Water, Environment and Health (UNU-INWEH), Ontario, Canada

CGIAR Research Program on Climate Change, Agriculture and Food Security (CCAFS)

Donors

This research study was funded by the following:

This work was implemented as part of the CGIAR Research Program on Climate Change, Agriculture and Food Security (CCAFS), which is carried out with support from CGIAR Fund Donors and through bilateral funding agreements. For details please visit *https://ccafs.cgiar.org/donors*. The views expressed in this document cannot be taken to reflect the official opinions of these organizations.

Contents

Acronyms and Abbreviations

ADPC	Asian Disaster Preparedness Centre
ALOS	Advanced Land Observing Satellite
APHRODITE	Asian Precipitation - Highly-Resolved Observational Data Integration Towards Evaluation of Water Resources
CC	Climate Change
CGIAR	A global research partnership for a food-secure future
CHI	Composite Hazard Index
CIESIN	Center for International Earth Science Information Network
CSI	Consortium for Spatial Information
DEM	Digital Elevation Model
DRR	Disaster Risk Reduction
EM-DAT	Emergency Events Database
EOSDIS	Earth Observing System Data and Information System
ESA	European Space Agency
ESRI	Environmental Systems Research Institute
GEBCO	General Bathymetric Chart of the Oceans
GFDRR	Global Facility for Disaster Reduction and Recovery
GIS	Geographic Information System
HDI	Human Development Index
IMD	India Meteorological Department
IPCC	Intergovernmental Panel on Climate Change
LST	Land Surface Temperature
MODIS	Moderate Resolution Imaging Spectroradiometer
NASA	National Aeronautics and Space Administration
NDDI	Normalized Difference Drought Index
NDVI	Normalized Difference Vegetation Index
NDWI	Normalized Difference Water Index
PALSAR	Phased Array type L-band Synthetic Aperture Radar
PSMSL	Permanent Service for Mean Sea Level
SAARC	South Asian Association for Regional Cooperation
SEDAC	Socioeconomic Data and Applications Center
SLR	Sea level rise
SRTM	Shuttle Radar Topography Mission
TRMM	Tropical Rainfall Measuring Mission
UNDP	United Nations Development Programme
UNISDR	United Nations International Strategy for Disaster Reduction
USD	United States Dollar
USGS	United States Geological Survey

Summary

All countries experience multiple climate-related risks that vary spatially and in time, and the combined impact of such risks may turn out to be very severe. To prioritize climate adaptation strategies, there is a need for quantitative, regional-level assessment of these risks. This report suggests methods for mapping such risks and estimating their impacts on people and agriculture in South Asia. Regional, country-wise and sub-national assessment of five climate-related risks – floods, droughts, extreme rainfall, extreme temperature and sea-level rise – is carried out. The approach involves overlaying climate hazard, sensitivity and adaptive capacity maps, and follows the vulnerability assessment framework of the Intergovernmental Panel on Climate Change (IPCC). A combined index based on hazard, exposure and adaptive capacity is introduced to identify areas susceptible to extreme risk.

The study presents a detailed and coherent approach to fine-scale climate hazard mapping that allows unambiguous identification of regions in South Asia which are most vulnerable to climate-related hazards. The study used data on the spatial distribution of various climate-related hazards in 1,398 sub-national areas of Bangladesh, Bhutan, India, Nepal, Pakistan and Sri Lanka. An analysis of country-level population exposure showed that approximately 750 million people are affected by combined climate hazards. Of the affected population, 72% is in India, followed by 12% each in Bangladesh and Pakistan. The remaining 4% is divided across Bhutan, Nepal and Sri Lanka. It was identified that agriculture was the most vulnerable sector due to its exposure to climate extremes, and that climatic upheavals had a direct impact on the economy of the country. An analysis of individual climate-related hazards indicates that floods and droughts affect agricultural areas the most, followed by extreme rainfall, extreme temperature and sea-level rise. Based on this vulnerability assessment, the regions that are most vulnerable to climate-related hazards in South Asia were identified - all the regions of Bangladesh; the Indian states of Andhra Pradesh, Bihar, Maharashtra, Karnataka and Orissa; Ampara, Puttalam, Trincomalee, Mannar and Batticaloa in Sri Lanka; Sindh and Balochistan in Pakistan; Central and East Nepal; and the transboundary river basins of Indus, Ganges and Brahmaputra.

Mapping Multiple Climate-related Hazards in South Asia

Giriraj Amarnath, Niranga Alahacoon, Vladimir Smakhtin and Pramod Aggarwal

Introduction

It is important to first list the terms and definitions that are used in this report. As defined by UNISDR (2009) and IPCC (2012), the basic components that should be considered in *risk* assessment are *hazard* and elements at risk, including their *exposure* and *vulnerability.* Hydrometeorological or *natural hazard* refers to a process or phenomenon of an atmospheric, hydrological or oceanographic nature that may cause loss of life, injury or other health impacts, damage to property, loss of livelihoods and services, social and economic disruption, or environmental damage (UNISDR 2009; IPCC 2012). Examples relevant to this report include floods, droughts, extreme rainfall, extreme temperature, and sea-level rise and are discussed in detail later.

Exposure refers to the presence, in *hazard* zones, of the elements at risk (e.g., people, infrastructure) that could be adversely affected and thereby subject to potential losses. Exposure is essentially a qualitative notion. Population exposure to hazard is defined, for example, as the likelihood that an individual in a given location is exposed to a given type of climate-related hazard over a certain period of time. *Vulnerability* refers to the characteristics and circumstances of a community, system or asset that make it susceptible to the damaging effects of a hazard (UNISDR 2009), i.e., predisposition of a community, system or asset to be adversely affected by a hazard. Vulnerability is, therefore, a measurable parameter. It can encompass economic, social, geographic, demographic, cultural, institutional, governance-related and environmental factors (IPCC 2012, 2014). Hence, measuring vulnerability is a complicated task and subject to interpretation. However, several authors strictly refer to the physical and environmental vulnerability (e.g., Cutter and Finch 2008; Kappes et al. 2012a; Pasini et al. 2012; Srinivasa Kumar et al. 2010), while others focus on the socioeconomic characteristics and damages (e.g., Orencio and Fujii 2014; Rufat et al. 2015; Füssell and Klein 2006; Malone and Engle 2011; Gallina et al. 2016).

Disaster is understood as a serious disruption of the functioning of a community or a society involving widespread human, material, economic or environmental losses and impacts, which exceeds the ability of the affected community or society to cope using its own resources (UNISDR 2009). Disaster is, therefore, seen primarily as an individual event – a realization of a hazard with a certain magnitude, extent and other parameters (unrelated to vulnerability). As hazard has varying degrees of severity through its realization in disasters, the more intense or severe the disaster, the greater is the potential for damage.

Finally, *risk* is understood as the probability that exposure to a hazard with a given vulnerability will lead to negative consequences. It is, therefore, quantified potential consequences of a hazard – potential loss of lives, health status, livelihoods, assets and services, which could occur within a particular community or society due to disaster over some specified future time period. Thus, a hazard poses no risk, if the system/community is not vulnerable (this is likely to be the case only when there is no exposure to that hazard, i.e., no presence of people and infrastructure in the hazard zone).

Related to this, disaster risk reduction (DRR) is the concept and practice of reducing risks by making systematic efforts to analyze and manage the causal factors of disasters, including through reduced exposure and vulnerability to hazards, and improved preparedness for disaster events. In this context, risk assessment is a methodology to determine the nature and extent of risk, by analyzing potential hazards and evaluating existing conditions of vulnerability that could together cause potential harm to people, property, services, livelihoods and the environment on which they depend (UNISDR 2009).

Extreme climate events regularly affect economic sectors and aspects of life, including agriculture, food security, water resources and health. The number of climate-related disasters (e.g., droughts, floods, landslides), globally, significantly increased in recent decades, from an average value of 195 per year (1987-1998) to 338 per year (2000-2011) (Guha-Sapir et al. 2012). In 2011, some 45% of recorded deaths and around USD 1,209 billion in economic losses were due to such disasters (Guha-Sapir et al. 2012). According to a World Bank report on the main hot spots of natural hazards (Dilley et al. 2005), about 3.8 million square kilometers (km^2) and 790 million people in the world are highly exposed to at least two climate-related hazards, while about 0.5 million km^2 and 105 million people are exposed to three or more hazards. Climate change (CC) further increases the exposure to multiple hazards, affecting their magnitude, frequency and spatial distribution (IPCC 2014).

At a global level, the World Bank initiated (Dilley et al. 2005) and Munich Re conducted (Touch Natural Hazards, www.munichre.com) a large-scale analysis of natural hazards, allowing a spatial visualization of hot spots where different hazards occur (e.g., floods, droughts, cyclones, earthquakes) using simple indices such as potential economic losses and human mortality. Such analyses are invaluable as global snapshots of the problem, but are normally not detailed enough to guide local DRR action.

In South Asia, interest in multi-risk assessment increased during the last decade, especially in relation to applications and initiatives aimed at the assessment of risks derived from different natural and man-made hazardous events (e.g., Scolobig et al. 2014; Kappes et al. 2012b). In Bangladesh, a recent study by the Asian Disaster Preparedness Centre (ADPC) supported by the national Disaster Management Agency identified, at sub-national level, hot spots where the population might be exposed to several hazards at the same time. For Nepal, a few studies supported by the Global Facility for Disaster Reduction and Recovery (GFDRR) of the World Bank, and the vulnerability assessment conducted by the International Water Management Institute (IWMI) at watershed level, mapped various hazards as well as the necessary interventions for risk reduction (ADPC 2010). Similar efforts in developing hazard and risk information in Sri Lanka were supported by the United Nations Development Programme (UNDP) (MoDM 2005). In India and Pakistan, most relevant studies have been confined to state/district level (Abid et al. 2016; Deen 2015; Kunte et al. 2014; Guleria and Patterson Edward 2012; Rafiq and Blaschke 2012; Saxena et al. 2013).

Overall, more detailed and robust assessments are required to actually guide DRR and CC adaptation investments at regional and sub-national scales, and to support climate justice principles that help distribute resources to states that are disproportionately impacted (Lerner-Lam 2007). The present study aims to contribute to filling this gap for the South Asia region. The objectives of this study are to:

- develop approaches for high-spatial-resolution mapping of areas exposed to several climate-related hazards: *floods, droughts, extreme rainfall, extreme temperature* and *sea-level rise*;
- develop a method for estimating the exposure of a population to individual natural hazards and their impacts on agriculture; and
- assess the overall vulnerability and risk at the country level based on country-wide, urban and rural population exposure to the five hazards above.

Data and Methods

Table 1 lists the main data sources used in the present study for the various hazards considered. Naturally, the assessment for different hazards had to be carried out at different spatial and temporal scales depending on the type of hazard, characteristics of the study area, and datasets publicly available.

TABLE 1. Details of datasets used for the mapping of climate-related hazards.

Hazard/feature	Dataset	Period	Spatial resolution	Temporal resolution	Source
Floods	Moderate Resolution Imaging Spectroradiometer (MODIS) surface reflectance product (MOD09A1)	2001-2013	500 m	8 days	National Aeronautics and Space Administration (NASA)[1]; Amarnath et al. 2012; Amarnath 2014a
Droughts	MODIS surface reflectance product (MOD09A1)	2001- 2013	500 m	8 days	NASA[1]; Amarnath 2014b
Extreme rainfall	Asian Precipitation – Highly-Resolved Observational Data Integration Towards Evaluation of Water Resources (APHRODITE)[2] and Tropical Rainfall Measuring Mission (TRMM)[3]	1951-2013	0.25 × 0.25 degrees (~27 km)	Daily	Yasutomi et al. 2011; NASA[3]
Extreme temperature	MODIS surface temperature	2001-2013	5,000 m	8 days	NASA[1]
Sea-level rise	Tidal gauge on sea-level rise	1930-2013	Point observations	Monthly	Permanent Service for Mean Sea Level (PSMSL)[5] and General Bathymetric Chart for the Oceans (GEBCO)[6]
Digital Elevation Model (DEM)	Shuttle Radar Topography Mission (SRTM)[4]	2000	90 m		Consortium for Spatial Information (CGIAR-CSI)
Socioeconomic and agricultural data	Gridded Population of the World, version 3 (GPWv3)	2010	2.5 × 2.5 degrees		Socioeconomic Data and Applications Center (SEDAC) (CIESIN 2005a, 2005b)[7]
	Agricultural land	2005	1,000 m		
	Human Development Index (HDI)	2012	Country-wise		Global land cover data (European Space Agency)[8] UNDP[9]

Notes:

[1] https://lpdaac.usgs.gov/dataset_discovery/modis/modis_products_table/mod09a1
[2] http://www.chikyu.ac.jp/precip/
[3] http://pmm.nasa.gov/data-access/downloads/trmm
[4] http://srtm.csi.cgiar.org/
[5] http://www.psmsl.org/data/
[6] http://www.gebco.net/
[7] http://sedac.ciesin.columbia.edu/data/collection/gpw-v3
[8] https://www.esa-landcover-cci.org/
[9] http://hdr.undp.org/en/data

Socioeconomic data from the Socioeconomic Data and Applications Data Center (SEDAC), operated by the Center for International Earth Science Information Network (CIESIN), a unit of the Earth Institute at Columbia University, and agricultural data from the European Space Agency (ESA) Global Land Cover were used to determine vulnerability and possible impacts of the five climate-related hazards considered in this study. The overall impact was determined by combining all individual hazard-specific assessments using a geographic information system (GIS) (Figure 1).

FIGURE 1. Conceptual approach and flowchart used for indicator-based assessment of climate-related hazards and identification of vulnerability hot spots.

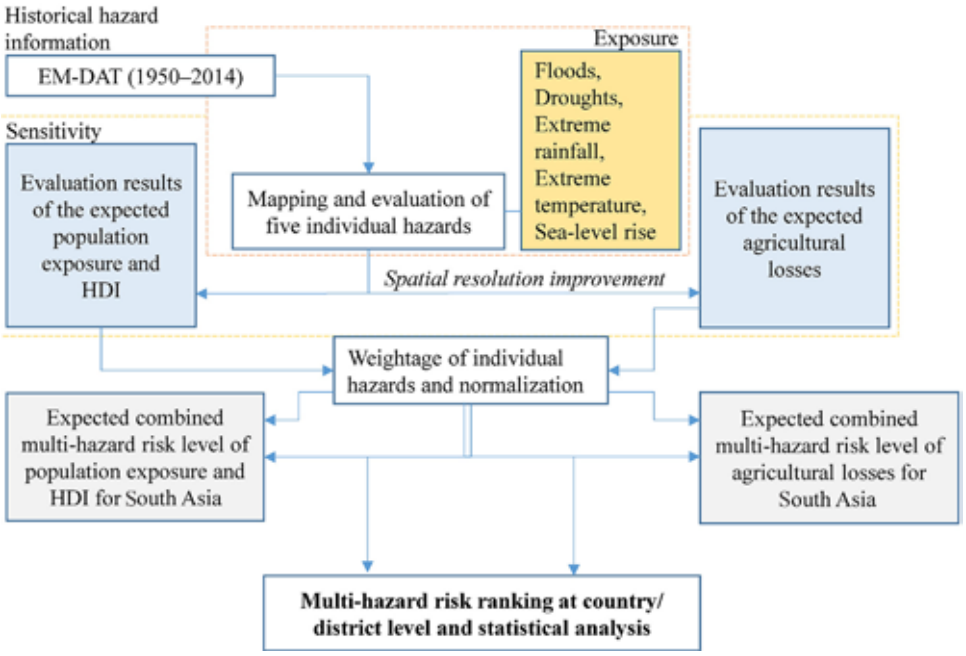

Floods

More than one-third of the world's land area is flood-prone, affecting about 82% of the global population (Dilley et al. 2005; Mosquera-Machado and Dilley 2009). According to EM-DAT (2015), about 3 billion people in more than 110 countries were affected by catastrophic flooding. Between 1980 and 2011, about 212,460 deaths were associated with floods worldwide. Destructive floods are common in tropical Asia (Kundzewicz et al. 2009).

Methods for mapping flood inundation and analyzing damage induced by floods include visual interpretation of satellite images (Jensen 2005), multi-spectral image classification (Sharma et al. 2011), band rationing (Jain et al. 2006), contextual multi-temporal classification and object-based classification (Cleve et al. 2008). In this study, the MODIS Surface Reflectance product (MOD09A1) (Sakamoto et al. 2007; Xiao et al. 2005) from the NASA's Earth Observing System Data and Information System (EOSDIS) was used. This product was available for the period 2001-2013, which translates into 46 8-day composite images annually, or over 500 composites in total. Each 8-day composite includes estimates of ground spectral reflectance of the seven spectral bands at 500 m spatial resolution. The flood inundation mapping algorithm, suggested by Amarnath et al. (2012) and verified against more resolute Advanced Land Observing Satellite Phased Array type L-band Synthetic Aperture Radar (ALOS PALSAR) (microwave) data, was used to identify water-related pixels (Figure 2) and classify them into temporary flooded or permanent water bodies in the context of land use and DEM.

A map of recurrently flooded areas in the South Asia region was prepared by overlaying each of the 8-day flood maps from 2001 to 2013 (Figure 3). Darker pixels in blue show areas that are severely affected by flooding in the Ganges-Brahmaputra-Meghna River Basin, and in the Indus River Basin.

FIGURE 2. (a) MODIS Terra satellite images, and (b) corresponding flood extent estimated using the flood inundation mapping algorithm of Amarnath et al. 2012.

(a) (b)

FIGURE 3. Spatial distribution of flood frequency based on 13 years' time series of MODIS imagery.

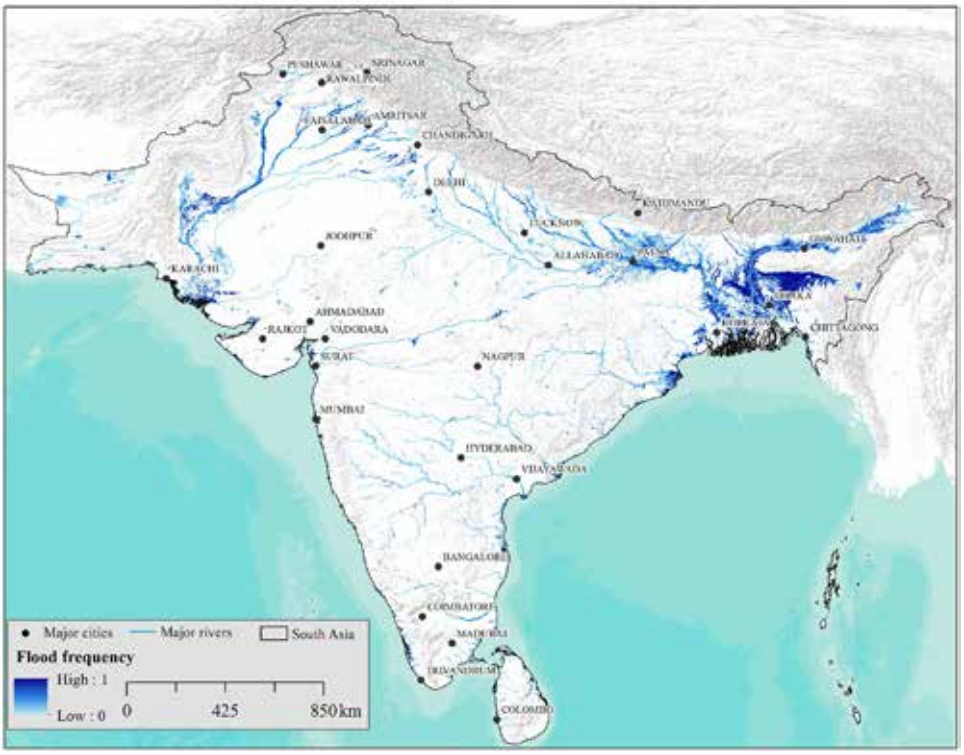

Droughts

Droughts are recurrent in South Asia, and their impacts on regional agriculture are enormous (SDMC 2010; Amarnath and Clarke 2016). The focus in this report is on meteorological and agricultural drought, characterized by rainfall deficit, declining soil moisture and consequent crop failure. During the period 2002-2003, South Asia faced one of the worst droughts, which was exceptional in terms of the magnitude, spatial extent and duration (Patel et al. 2007, 2012; Dutta et al. 2013). In India alone, a drought has been reported at least once in every 3 years in the last five decades (Mishra and Singh 2009; UNISDR 2009). The country incurred financial losses of about USD 149 billion and approximately 350 million people were affected due to droughts in the past 10 years (Gupta et al. 2011; SDMC 2010). Traditionally, most meteorological departments in South Asia monitor droughts using observations at weather stations. Such point observations, although useful, have limited ability to trace the spatial extent and dynamics of the drought (http://www.imdpune.gov.in/Clim_Pred_LRF_New/Products.html). Such spatial and continuous view is provided by remote sensing technology with the use of various drought-related indices.

A number of drought-related indices have been applied for drought monitoring in recent decades (Bhuiyan et al. 2006; Brown et al. 2008; Dutta et al. 2013; Gebrehiwot et al. 2011; Ghulam et al. 2007; Kogan 1995; Mishra and Singh 2009; Rhee et al. 2010; Thenkabail et al. 2004; Qin et al. 2008; Zargar et al. 2011). Gu et al. (2007) developed the Normalized Difference Drought Index (NDDI), which can be used to assess drought by combining the Normalized Difference Vegetation Index (NDVI) and the Normalized Difference Water Index (NDWI) (Gouveia et al. 2012).

$$NDVI = \frac{p857 - p645}{p857 + p645} \quad (1)$$

$$NDWI = \frac{p857 - p2130}{p857 + p2130} \quad (2)$$

where: ρ857, ρ645 and ρ2130 are the surface reflectance of 857, 645 and 2130 nanometer (nm) wavelengths, respectively. Both indices range from 0 to 1. NASA's MODIS Surface Reflectance data from 8-day composite images from 2001 to 2013 (MOD09A1 with 500 m spatial resolution) were used to calculate NDVI (Equation [1]) and NDWI (Equation [2]) to determine the vegetation-water stress and to calculate NDDI (Equation [3]). The product quality assessment (QA) flags in the MOD09A1 products provide information about different types of atmospheric noise. For each 8-day period, a visual quality control in ArcGIS was made, of which the different QA values detected the cloud cover in the data period. After removing the clouds from the dataset, the next step was to replace the cloudy pixels with values as realistic as possible. NDVI and NDWI were then calculated from the MOD09Q1 dataset, and clouds were removed with the cloud mask. From these clear-sky, time-series of reflectance values, we calculated 13-year NDVI and NDWI values for each 8-day step during the period 2001-2013.

$$NDDI = \frac{NDVI - NDWI}{NDVI + NDWI} \quad (3)$$

NDDI captures areas that are subject to water and vegetation stress due to a delay in the onset of the summer monsoon, which generally occurs from June to September. NDDI is, therefore, a more sensitive indicator of drought in cropland than NDVI alone. NDDI varies in the range of 0 to 1. In the current study, a pixel was categorized as being under drought if NDDI was greater than 0.6 and as non-drought otherwise (based on a comparison of NDVI and NDWI in drought years and supported by similar studies elsewhere - Gu et al. 2007; Liu and Wu 2008). For mapping purposes, the drought and non-drought pixels were assigned values 1 and 0, respectively. At the final step, all individual 8-day maps of drought/non-drought conditions were combined in ArcGIS, and a number of cases where a drought was detected in any pixel over the study period were calculated. The final map was produced by normalizing the counts from 0 to 1, where 0 means 'no drought was ever detected in a pixel over the study period' and 1 is 'drought was detected in a pixel continuously' (Figure 4).

FIGURE 4. Spatial distribution of drought frequency based on 13 years' time series of MODIS imagery.

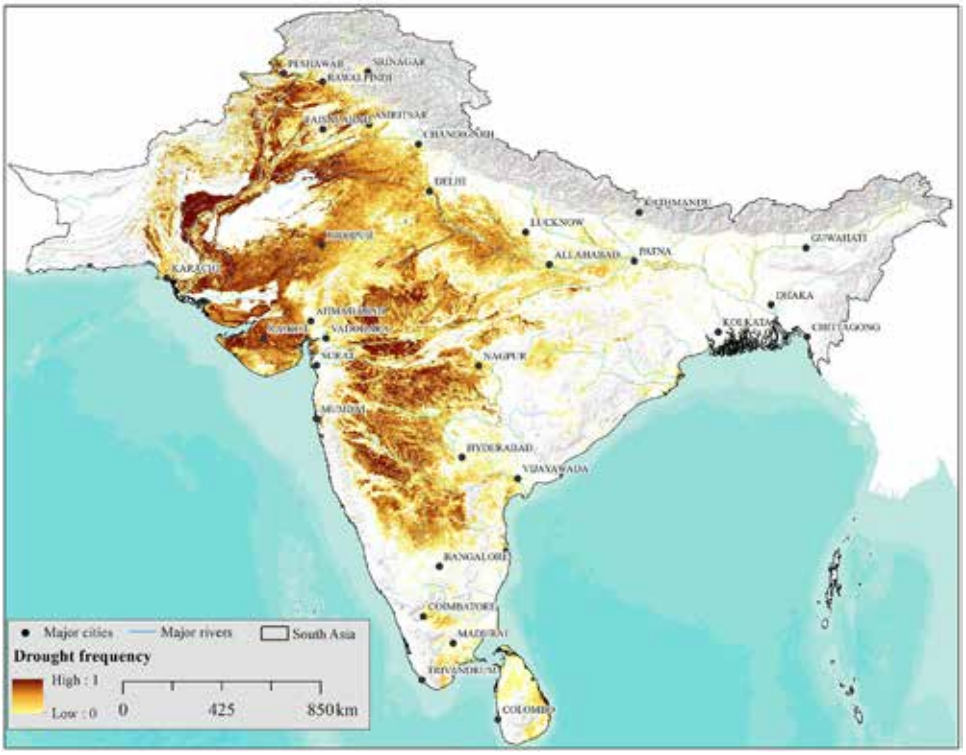

Extreme Rainfall

Extreme rainfall leads to crop failure, soil erosion, landslides, and may be a precursor of flash floods and inundation. Understanding and quantifying extreme rainfall events are critical to improving community resilience (Pattanaik and Rajeevan 2010; Guhathakurta and Rajeevan 2006). Classification of rainfall events by the India Meteorological Department (IMD) for daily rainfall extremes (Table 2) was used to determine extreme rainfall zones for the entire region. Long-term rainfall records from two major data sources (APHRODITE for the period 1951-2007 and TRMM for the period 2008-2013), covering a time frame of 62 years in total, were used to identify areas of extreme rainfall. Both APHRODITE and TRMM were used to examine the frequency of rainfall events for the three categories shown in Table 2, during the monsoon season in the months of June, July, August and September. The average frequency of each category during these months was calculated by adding the total number of rainfall events for each category in a particular grid cell for a given year. The total number of events from each grid cell is added for the entire region to obtain the total number of such events in South Asia.

TABLE 2. Categorization of observed rainfall for classification of extreme rainfall events.

Rainfall categories	IMD classification of rainfall events	Rainfall (R), mm day^{-1}
Category 1 (low)	Light to somewhat heavy	R <= 64.4
Category 2 (medium)	Heavy	64.4 < R <= 124.4
Category 3 (extreme)	Very heavy to exceptionally heavy	124.4 < R

Source: India Meteorological Department.

Figure 5 shows that the average frequency of extreme rainfall of categories 1 (low) and 3 (extreme) exhibit an increasing trend (ρ values of 0.05), whereas category 2 (medium) exhibits a slightly decreasing trend during the monsoon season. This result is also consistent with a previous study on the spatial and temporal variability of rainfall events in India, which suggested a threshold value of 124.4 mm day^{-1} of rainfall as a threshold for extreme rainfall (category 3) in this region (Pattanaik and Rajeevan 2010).

FIGURE 5. Average frequency of rainfall events during the monsoon season (June to September) from 1951 to 2013 for the entire South Asia Region in three categories – (a) 1 (low), (b) 2 (medium), and (c) 3 (extreme).

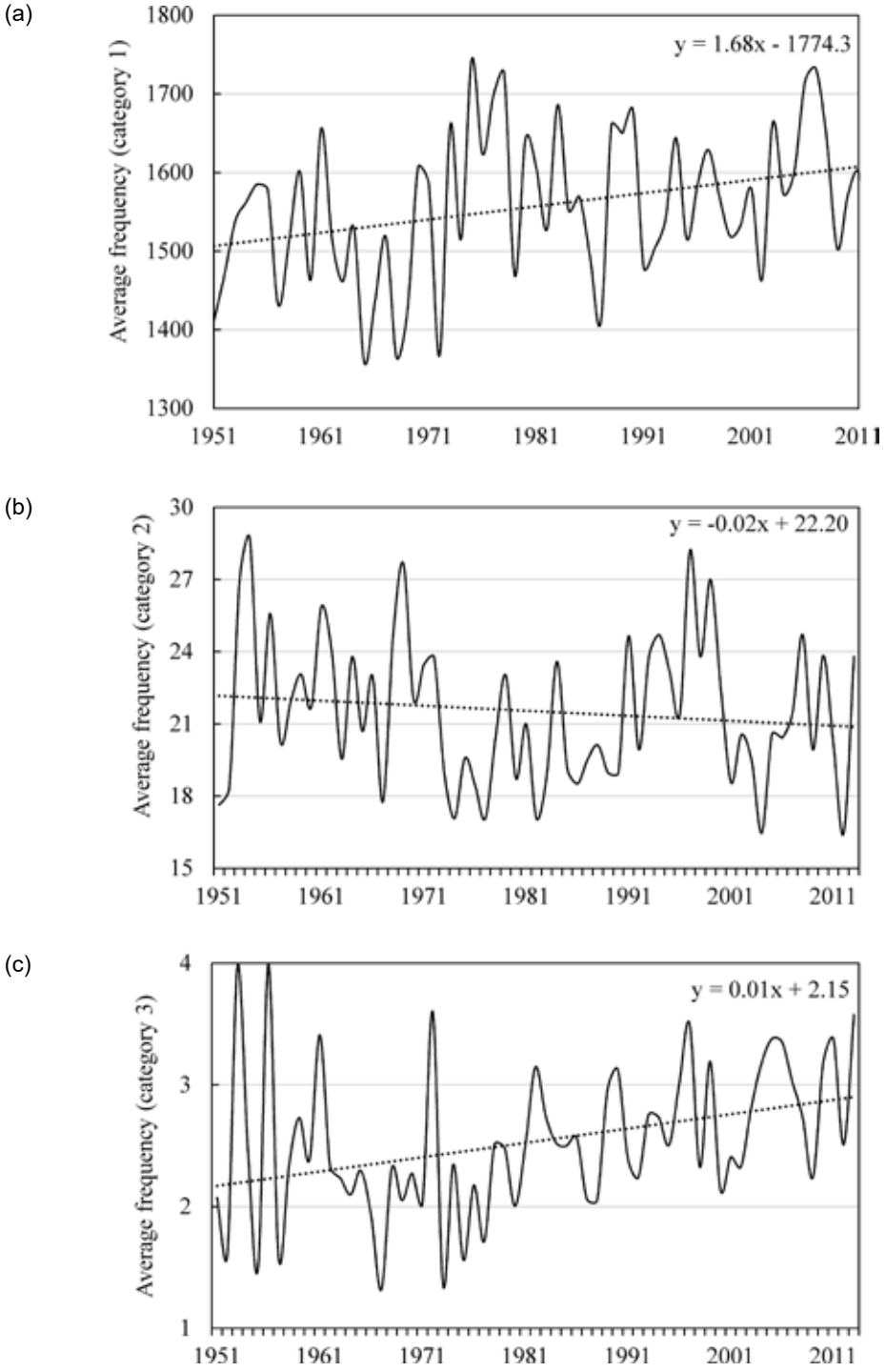

The procedure followed for characterizing spatial rainfall patterns was as follows: when the daily rainfall value exceeds a threshold of 124.4 mm, those pixels on the rainfall grid map were classified as 1 and otherwise 0. The same process was applied for each set of satellite-based daily rainfall data. These binary maps were overlaid to compute the frequency of extreme rainfall in pixels over the study period from 1951 to 2013. Higher recurrence was pointed to high rainfall hazard, while lower recurrence to low hazard. The final dataset of extreme rainfall was normalized to a 0-1 scale.

The above procedure provided the spatial coverage of extreme events with a spatial resolution of 0.25° (approximately 27 km). More resolute extreme rainfall data are crucial for practical applications. Rainfall is related to variables such as topography and vegetation (Badas et al. 2005; Onema and Taigbenu 2009). The resolution of remote sensing data for these variables is higher. For example, the resolution of MODIS NDVI, a proxy of vegetation, has reached 500 m by now. The spatial resolution of extreme rainfall map can, therefore, be improved by examining a relationship of rainfall with such variables (Figure 6). Immerzeel et al. (2009) improved the resolution of rainfall to 1 km by establishing such an exponential relationship between NDVI and TRMM. The present study used the geostatistical downscaling procedure of Immerzeel et al. (2009) to develop a final, high resolution (500 m) spatial product. Figure 7 is an example of a scatter plot of NDVI and rainfall in the Tangail District of Bangladesh, a region which is characterized as an extreme rainfall zone (category 3, Table 2). The figure illustrates the high correlation between NDVI and rainfall (0.93). In the creation of Figure 7, 8-day NDVI data for the months from June to September were layer-stacked and correlated with a satellite rainfall product to downscale it to 500 m. Figure 8 presents the final, high-resolution extreme rainfall hazard map, which was developed using the geostatistical downscaling procedure of Immerzeel et al. (2009).

FIGURE 6. The time series of NDVI and rainfall for Tangail District in Bangladesh, illustrating the pattern of dependency of NDVI on rainfall.

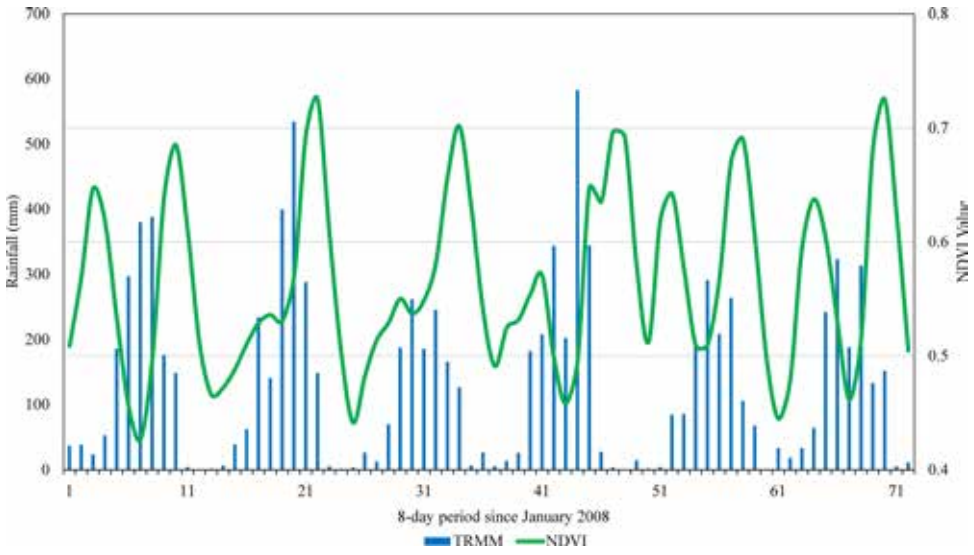

FIGURE 7. Scatter plot illustrating the relationship between extreme rainfall and average NDVI values for Tangail District in Bangladesh.

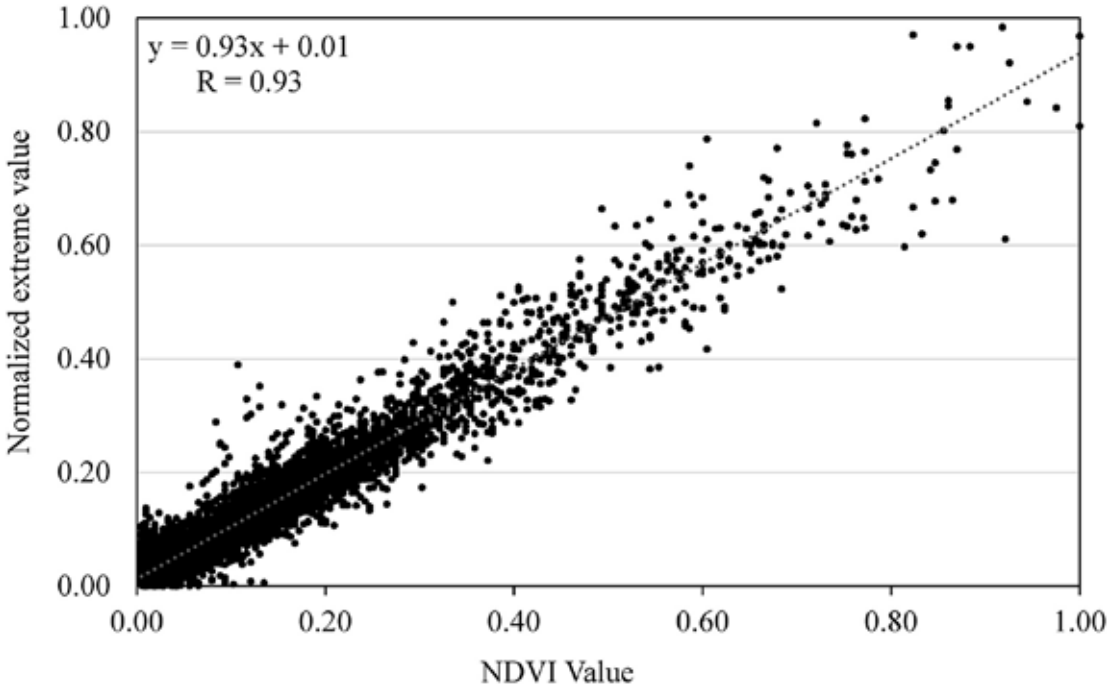

FIGURE 8. Spatial distribution of extreme rainfall frequency based on 62 years' time series of APHRODITE and TRMM rainfall datasets.

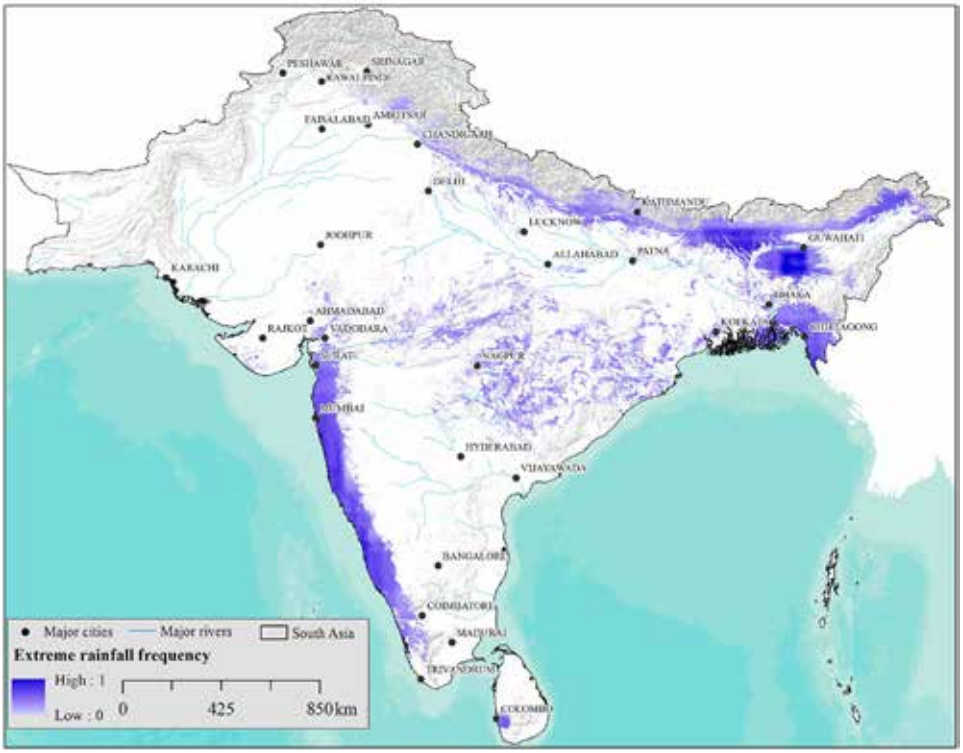

Extreme temperature

A heat wave (extreme temperature) is a prolonged period of abnormally hot weather. With an overall warming of the Earth's climate, heat waves are expected to become more frequent, longer and more intense in places where they already occur (IPCC 2014). An increase in the frequency and severity of heat waves can lead to crop failure, increased livestock mortality, increased human illnesses and deaths, and power outages. Naturally, countries which are located closer to the equator have a higher risk of heat waves than those further away. Therefore, this is another major climatic hazard for the South Asia region. Heat waves are analyzed here only for the pre-monsoon season, because the impacts are likely to be experienced during that time of the year (Murari et al. 2015). Extreme temperatures associated with heat waves occur in South Asia in the second half of May and early June, reaching 40-45 °C in most of the heat-stressed hot spot areas.

To analyze the heat wave hazard, MOD11C2 data from 2000 to 2013, composited for 8-day periods, were used. MODIS land surface temperature (LST) data are based on the generalized split-window algorithm (Wan and Dozier 1996) and day/night algorithm (Weng et al. 2004), which resolve ambiguities arising from variable emissivity and are accurate to within 1 °C in most cases (Wan 2008, 2014). The summer windows from day-of-year 55 to 154 (late-February to early-June) for MOD11C2 were chosen based on correlation between temperature and NDWI (Figure 9). Data with poor calibration, cloud contamination or other quality issues were excluded based on the LST product quality assurance flags provided.

The MODIS-based LST anomaly products represent both higher and lower temperature variations from 0 to -12 °C and 0 to +12 °C, respectively, as shown in Figure 10. To map the heat wave hazard, only the highest temperature variations are considered; lower values in the range of 0-6 °C are not hazardous. For each pixel and each 8-day time period, the 2008-2013 mean values were subtracted to obtain temperature anomalies. When the temperature anomaly value was greater than 6 °C, pixels were classified as 1 and otherwise as 0. All 8-day binary maps for the months from April to June were overlaid to calculate the frequency of a high temperature anomaly. Images were projected into a world cylindrical equal-area projection with 5 km × 5 km cells, which is approximately equivalent to the 0.05° × 0.05° resolution of the MODIS products.

FIGURE 9. Time series of land surface temperature and NDWI from February to May in Rajkot Taluk of the Gujarat State, India.

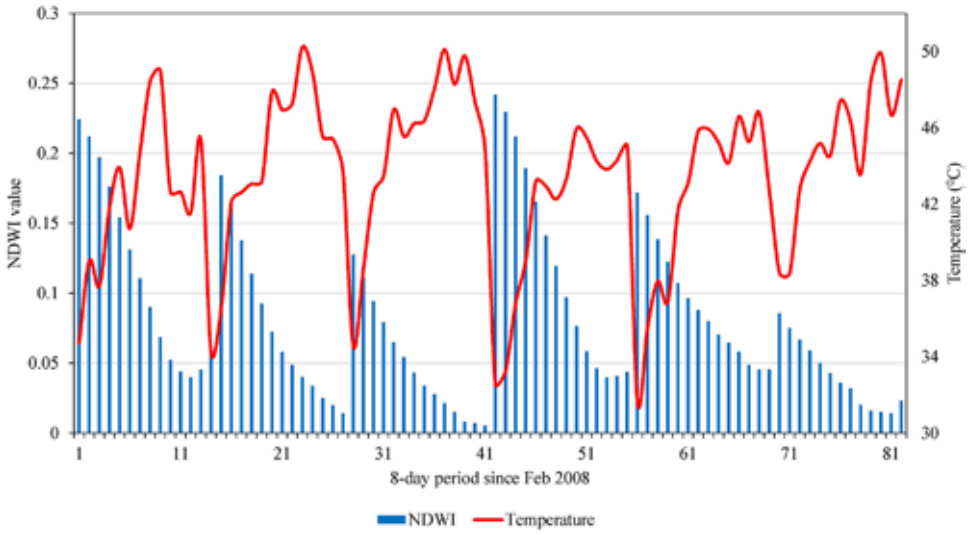

To downscale the 5 km heat wave data into a 500 m spatial resolution, an approach similar to that of downscaling extreme rainfall was used (Figure 11). The frequencies were then normalized to 0-1 scale. The resulting heat wave hazard map is illustrated in Figure 12.

FIGURE 10. Land surface temperature (LST) anomalies for South Asia from (a) June 2 to 9, 2014, and (b) June 10 to 17, 2014.

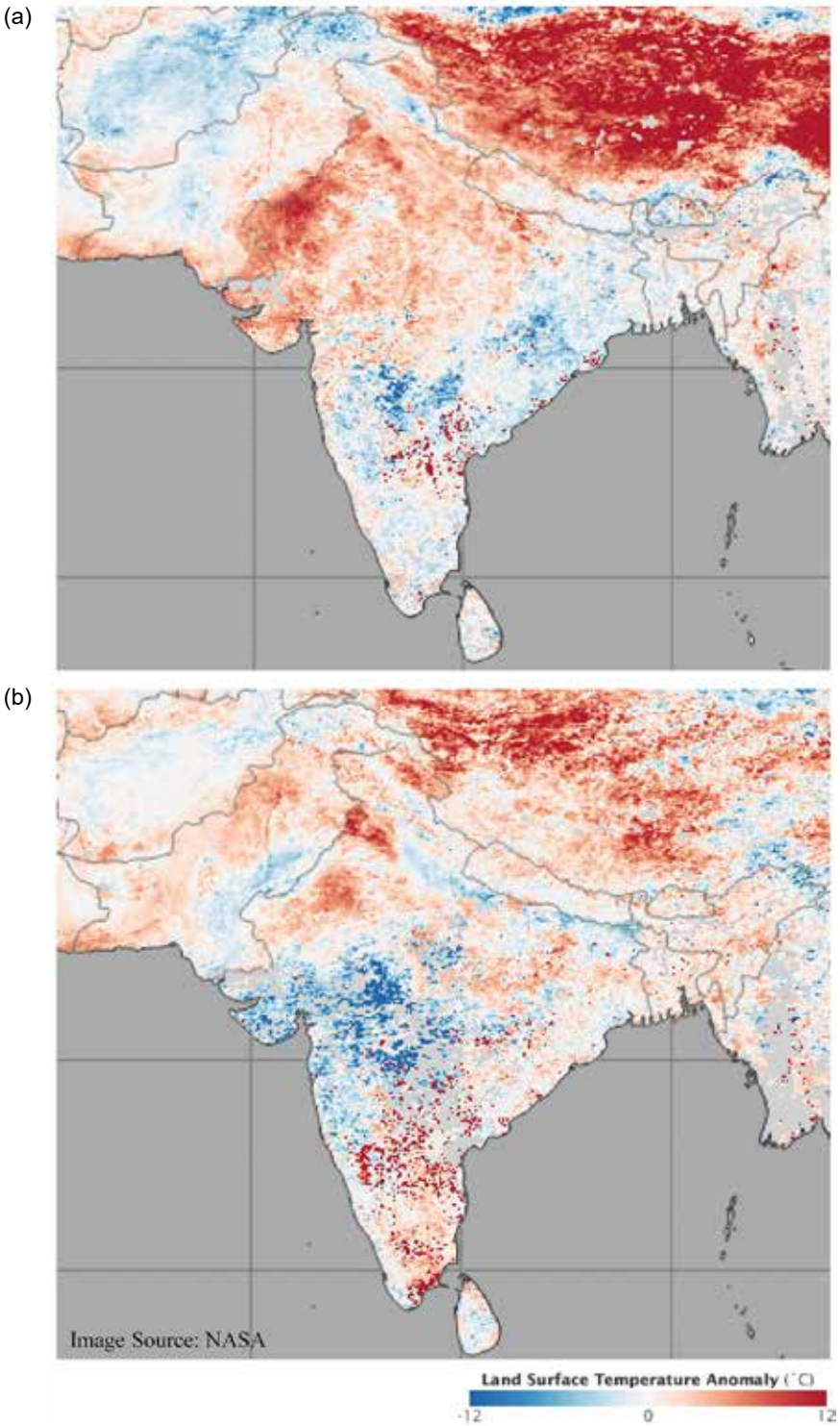

Notes: LST anomalies are not absolute temperatures; instead, they show how much the land surface was heated above or below the average. The darkest red areas are those where the ground was as much as 12 °C above the normal value from 2001 to 2010; blue areas show where it was below the normal value; and grey areas highlight where there were incomplete data (usually due to excessive cloud cover).

FIGURE 11. Scatter plot illustrating the relationship between normalized extreme heat and NDWI values.

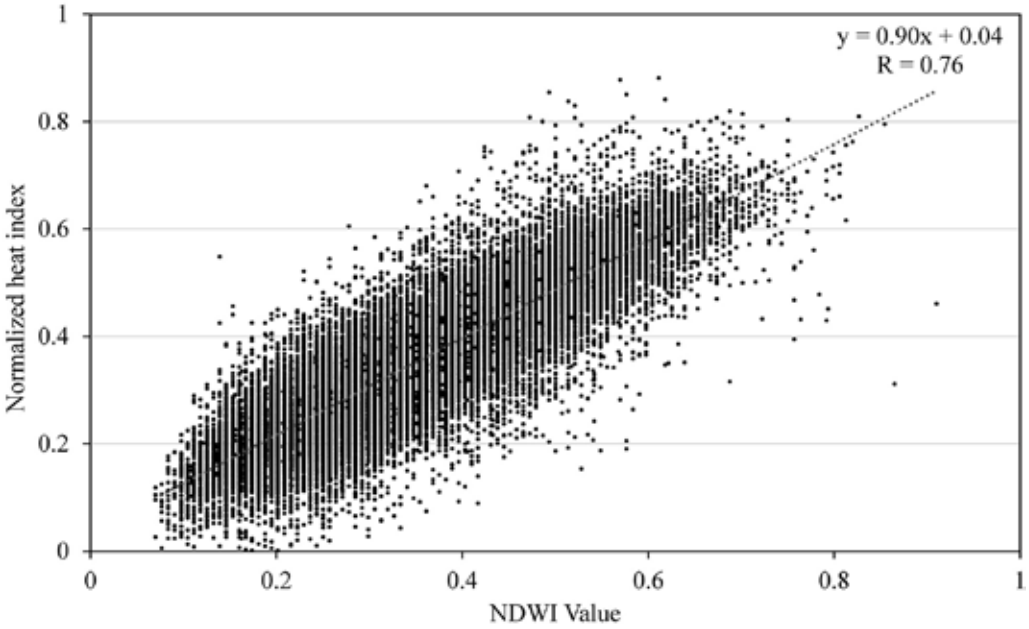

FIGURE 12. Spatial distribution of the frequency of extreme temperature/heat waves.

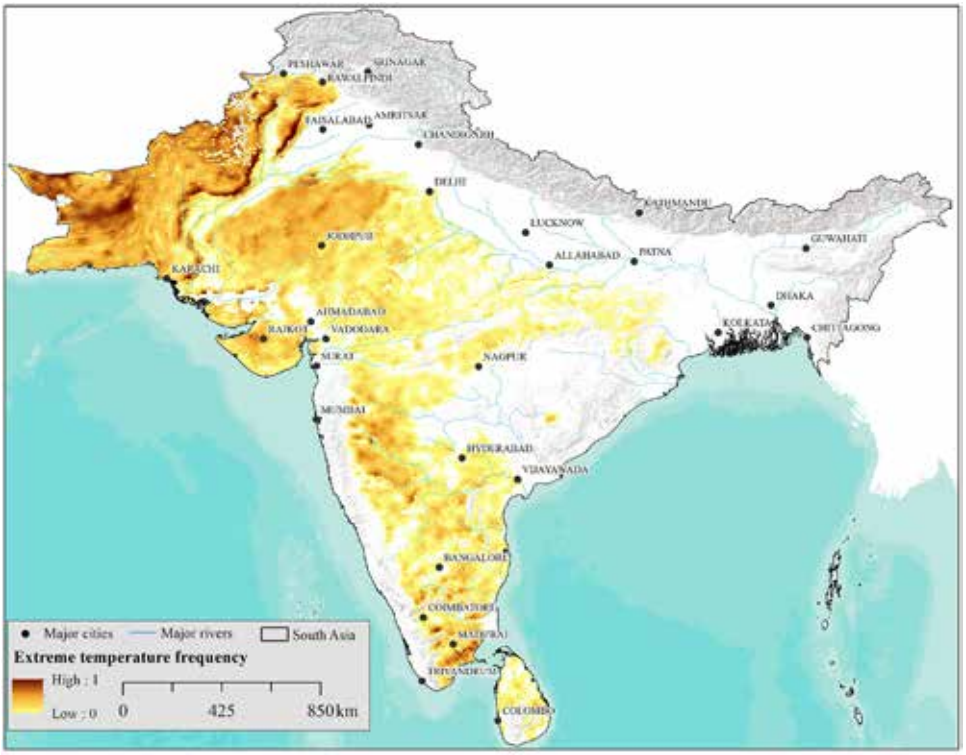

Sea-level Rise

Accelerated sea-level rise (due to global climate change) is likely to increase the risk of coastal zone flooding by way of storm surges, tsunamis and severe wave processes (Mani Murali et al. 2013). Population density in the coastal zones of South Asia has increased drastically during the last 15 years, and this has led to a further increase in risk due to natural hazards (Mani Murali et al. 2013). To date, the coastal hazard assessments were carried out at Puducherry and Cuddalore in South India (Mani Murali et al. 2013; Saxena et al. 2013), western Bangladesh (Karim and Mimura 2008) and the Indus Delta in Pakistan (Salik et al. 2015). In this study, mapping of this hazard along the South Asian coast was carried out by integrating the following six different parameters:

- Rate of sea-level rise
- Coastal slope
- Regional elevation
- Tidal range
- Tsunami wave arrival height
- Coastal geomorphology

Rate of Sea-level Rise

Mean sea level can be defined as the seawater height with respect to a reference benchmark. Measurements of changes in sea level in South Asia are based on a total of 18 tidal gauge stations (Figure 13) obtained from the PSMSL (www.psmsl.org) program. By using PSMSL stations, tidal data on the annual rate of sea-level rise were calculated by establishing the trend of sea-level change between seawater height and time for each station. As an example, Figure 14 shows the monthly changes in sea level in India within a 988-month (1914 to 2013) period. The trend line of monthly sea-level change is used to calculate the annual sea-level change (mm yr^{-1}). In each case, the trend line was found to be statistically significant at the 5% level using a student's t-test on each regression estimate of the trend coefficient. The annual rate of sea-level rise for all 18 tidal gauge stations was interpolated to generate a map showing the rate of sea-level rise for the entire South Asian coastline.

FIGURE 13. Locations of tidal gauge stations (blue circles) on the South Asian coastline.

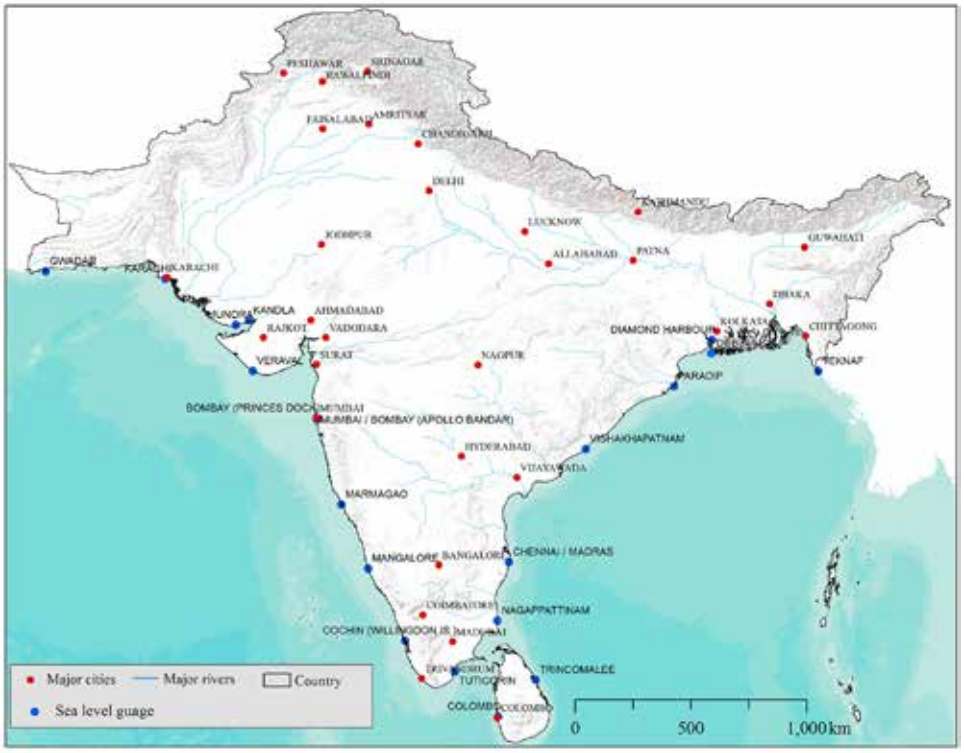

FIGURE 14. Time series of sea-level change at (a) Dublakhal, and (b) Nagappattinam tidal gauge stations.

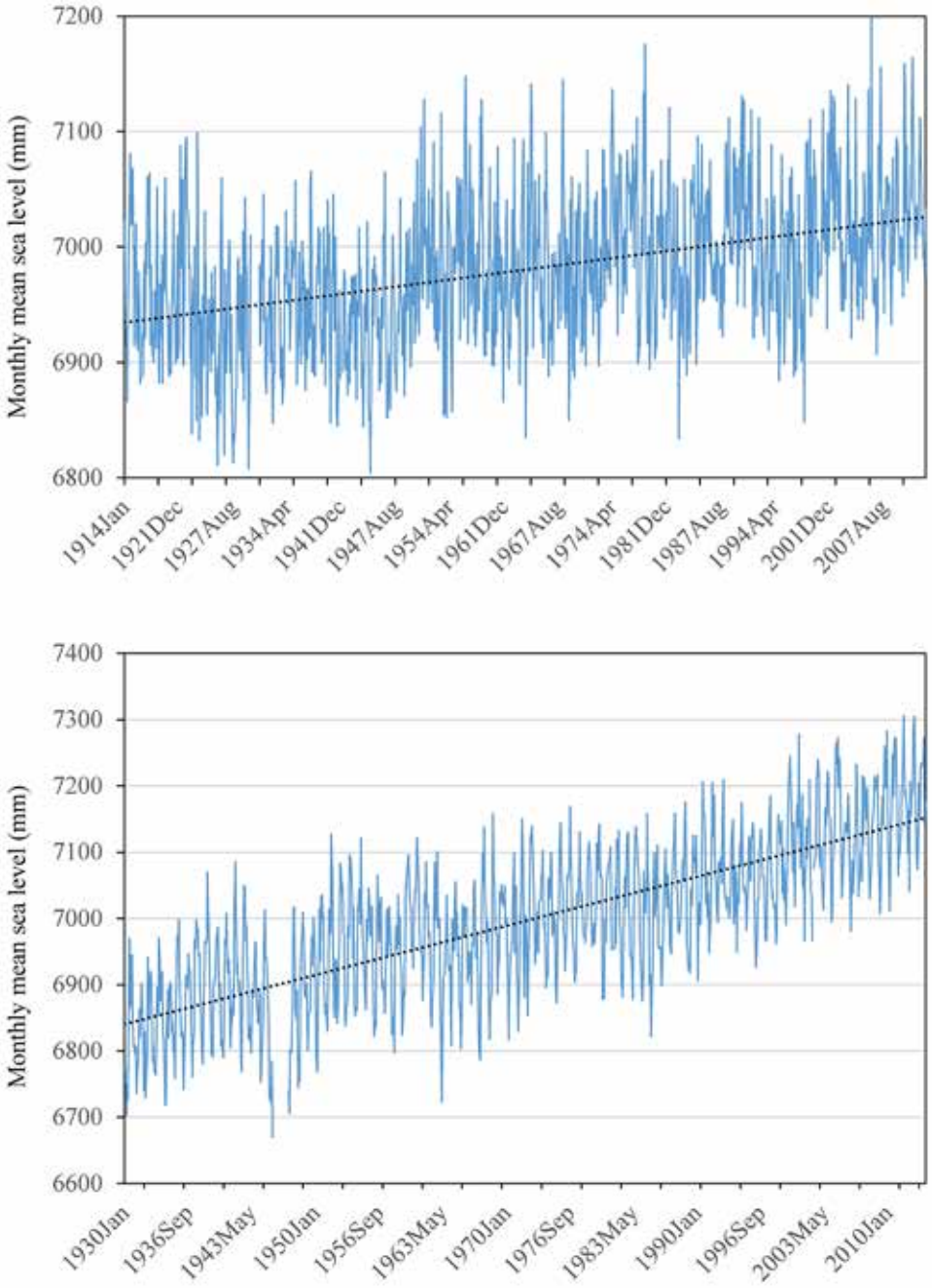

Coastal Slope

Coastal slope is defined as the ratio of altitude change to the horizontal distance between any two points on the coast. Coastal slope is linked to the susceptibility of a coast to inundation by flooding (Thieler 2000). The run-up of waves on a coast is the most important stage of a tsunami from the viewpoint of evaluating the level of tsunami hazard for the coast (Dotsenko 2005). Coastal slope is an important parameter in deciding the degree to which coastal land is at risk of flooding from storm surges and during a tsunami (Sterr et al. 2000). Coastal locations having gentle land slope values have great penetration of seawater compared to locations with fewer slopes, and resulting land loss from inundation is simply a function of slope: the lower the slope, the greater the land

loss (Sterr et al. 2000). Thus, coastal areas having gentle slope values were considered as more vulnerable areas, and areas with steep slopes as areas of low vulnerability. The methodology was adopted from the previous studies carried out in coastal areas of India (Mani Murali et al. 2013; Srinivasa Kumar et al. 2010).

GEBCO data of one-minute grid resolution coastal topography and bathymetry were used to obtain the regional slope of the coastal area. The data also incorporates land elevations derived from the Global Land One-kilometer Base Elevation (GLOBE) project datasets. A 90 m SRTM DEM was also used. GEBCO data are useful in deriving the coastal slope values on both land and ocean. The slope values (in degrees) are calculated using the Environmental Systems Research Institute (ESRI) ArcGIS tool.

Regional Elevation

Regional elevation is referred to as the average elevation of a particular area above mean sea level. From the vulnerability perspective, higher elevation values will be considered as being less vulnerable to future sea-level rise, because such elevation provides more resistance to inundation due to rising sea level or storm surges. Coastal areas with low elevation are considered to be highly vulnerable to sea-level rise.

Tidal Range

Tidal range is the vertical difference between the highest high tide and the lowest low tide, and coastal areas with a high tidal range are characterized as highly vulnerable. For the current study, data from WXTide software (http://www.wxtide32.com/) for the year 2011 were used as a base to calculate the predicted tidal range. Altogether, 18 stations were used to analyze average tidal range, and assign high tidal range for highly vulnerable areas and low tidal range for less vulnerable areas.

Tsunami Wave Arrival Height

Tsunamis can cause flooding due to the intrusion of seawater up to 1 km inland or even further. Based on previous studies (Mani Murali et al. 2013; Srinivasa Kumar et al. 2010), the risk ratings were assigned to predict the run-up heights and travel times of a tsunami wave at different parts of the coastline.

Coastal Geomorphology

Coastal geomorphology is yet another parameter that determines how vulnerable the coastline is to sea-level rise caused by CC. Landsat TM and ETM+ satellite images, and a Digital Terrain Model were used to describe the coastal geomorphology. The geomorphologic classes were defined based on visual interpretation with a coastal zone of 1 km to identify major classes that include sandy beaches, inundated coast, cliffs, estuaries, mangroves, salt pans, etc. Further, these geomorphologic classes were assigned a risk rating as high vulnerability (sandy beaches, deltas, mangroves, salt pans), moderate vulnerability (estuaries) and low vulnerability (inundated coast and cliffs).

Composite Sea-level Rise Hazard Index

Each of the six parameters described has been categorized into low to high classes and ranked as shown in Table 3. The total rank (R) of all six hazard parameters was calculated as a sum of the rank given to individual parameters (Equation [4]), assuming that all parameters make an equal contribution.

$$R = Rr + Rc + Re + Rt + Rs + Rg \quad (4)$$

Where: Rr is the rank of the rate of sea-level rise, Rc is the rank of coastal slope, Re is the rank of regional elevation, *Rt* is the rank of tidal range, *Rs* is the rank of tsunami wave arrival height and *Rg* is the rank of coastal geomorphology. The six parameter map layers were then overlaid and the final normalized composite sea-level rise (SLR) hazard index was calculated using Equation (5).

$$SLR = (R - Rmin) / (Rmax - Rmin) \quad (5)$$

where: Rmin and *Rmax* are minimum and maximum values of the total hazard ranks, respectively. SLR ranges between 0 and 1, as for all other hazards described in earlier sections. Figure 15 shows the final map of the composite index for sea-level rise (SLR) hazard.

TABLE 3. Ranks of six different parameters used in the mapping of sea-level rise.

Parameter	Hazard rating		
	Low (1)	Medium (2)	High (3)
Rate of sea-level rise (mm yr^{-1})	<= 0.5	> 0.5 and <= 1.0	> 1.0
Coastal slope (degrees)	> 1.0	> 0.2 and <= 1.0	>= 0 and <= 0.2
Regional elevation (m)	> 6.0	> 3.0 and <= 6.0	>= 0 and <= 3.0
Tidal range (m)	<= 2.5	> 2.5 and <= 3.5	> 3.5
Tsunami wave arrival height (m)	>= 0 and <= 1.0	> 1.0 and <= 2.0	> 2.0
Geomorphology	Inundated coast, cliffs	Estuaries, vegetated coast	Sandy beaches, deltas, mangroves, salt pans

FIGURE 15. Composite index for sea-level rise (SLR) hazard.

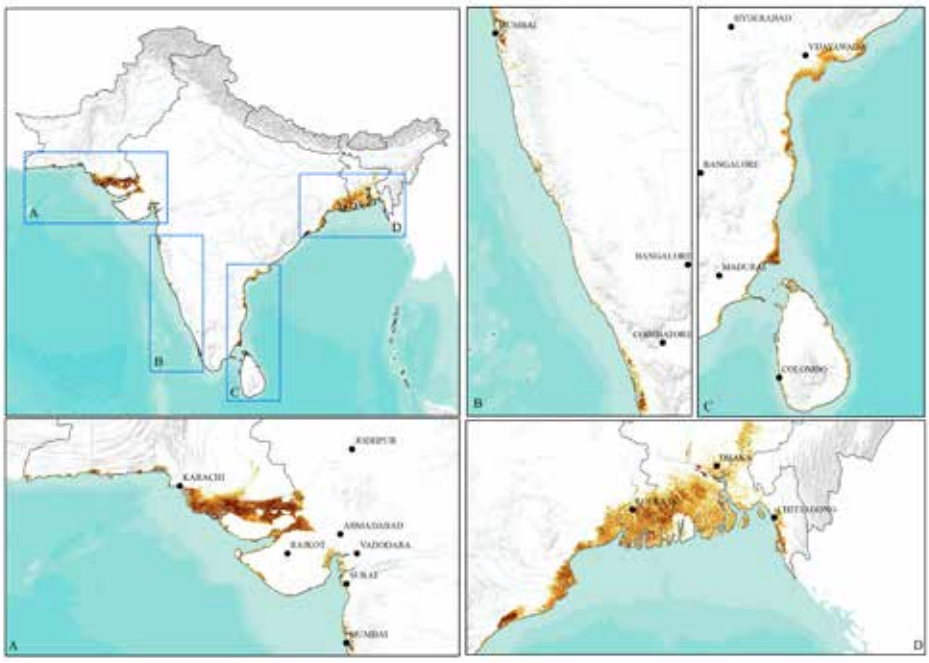

Combined Hazard Index (CHI)

Each of the individual hazards – floods, droughts, extreme rainfall, heat waves and sea-level rise – is classified initially into hazard and non-hazard areas to calculate the frequency of multi-hazard for a given pixel using Equation (6).

$$CHI = \frac{xi - (xi)min}{(xi)max - (xi)min} \quad (6)$$

where: CHI is the standardized hazard of type *i*, *Xi* is the non-standardized hazard of type *i*, and $(Xi)_{min}$ and $(Xi)_{max}$ are the minimum and maximum values, respectively, of the i^{th} hazard.

Indicator maps were then overlaid to calculate the overall hazard score by summing the above binary data for each pixel. A score between 1 and 5 indicates the number of times a particular hazard occurred. The resulting multi-hazard map is shown in Figure 16, with a few enlarged windows for better visibility.

FIGURE 16. Maps showing exposure to multiple hazards across Bangladesh, Bhutan, India, Nepal, Pakistan and Sri Lanka.

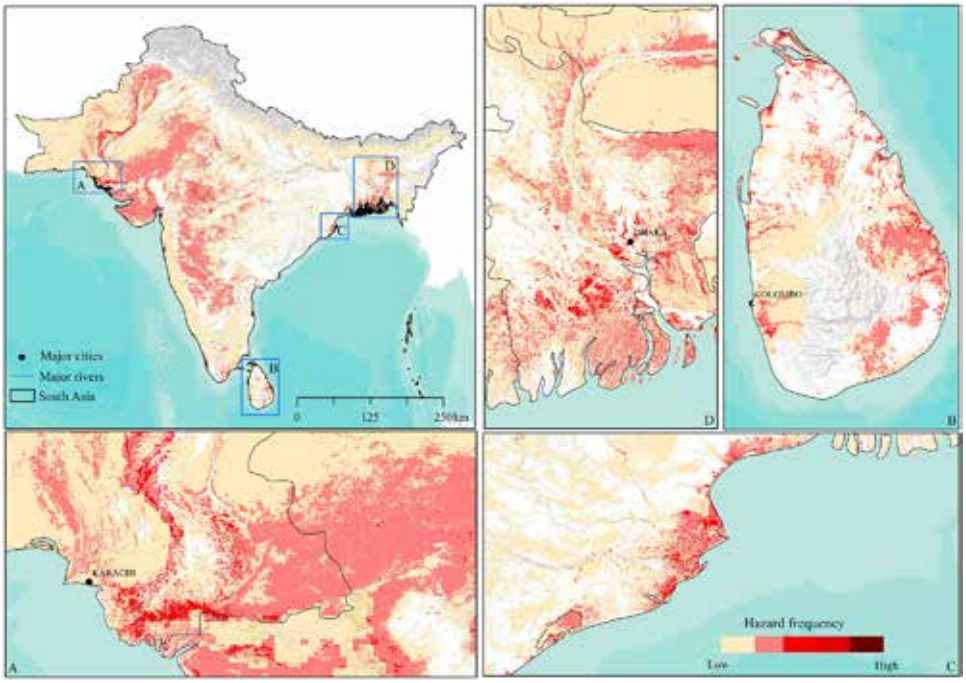

Note: The darker the color, the higher the number of hazards experienced in that area.

Population Exposure

Population exposure scores for each grid cell were calculated separately for floods, droughts, extreme rainfall, heat waves and sea-level rise. The population count in each cell (*Pop*count*cell*) was multiplied by the likelihood of that cell experiencing an individualclimate hazard (*H*). For example, for the drought hazard, the population exposure score is shown in Equation (7).

$$Cell\ \text{Exposure}_{drought} = Popcount_{cell} \times H_{drought,\ cell} \quad (7)$$

As shown in Equation (8), a cell's exposure to multiple climate hazards is determined by summing the values of exposure to individual hazards. The types of hazard events were weighted equally.

$$Cell\ \text{Exposure}_{multi\text{-}hazard} = Popcount_{cell} * \sum (H_{floods} + H_{droughts} + H_{extreme\ rainfall} + H_{extreme\ temperature} + H_{sea\text{-}level\ rise}) \quad (8)$$

Population exposure to each climate hazard is shown in Figure 17. Figure 18 shows population exposure to multiple climate hazards in eastern India and Bangladesh.

Population exposure to individual and multiple climate hazards was calculated at incremental scales, at city, district and national level based on the respective extents. The cell exposure values within each geographical boundary of urban, rural and country extents under consideration were summed over the study region to calculate the average population exposure scores. Further, exposure of each country/region to individual and multiple hazards was derived from the resultant dataset.

FIGURE 17. Population exposure to individual climate hazards – floods, droughts, extreme rainfall, heat waves and sea-level rise.

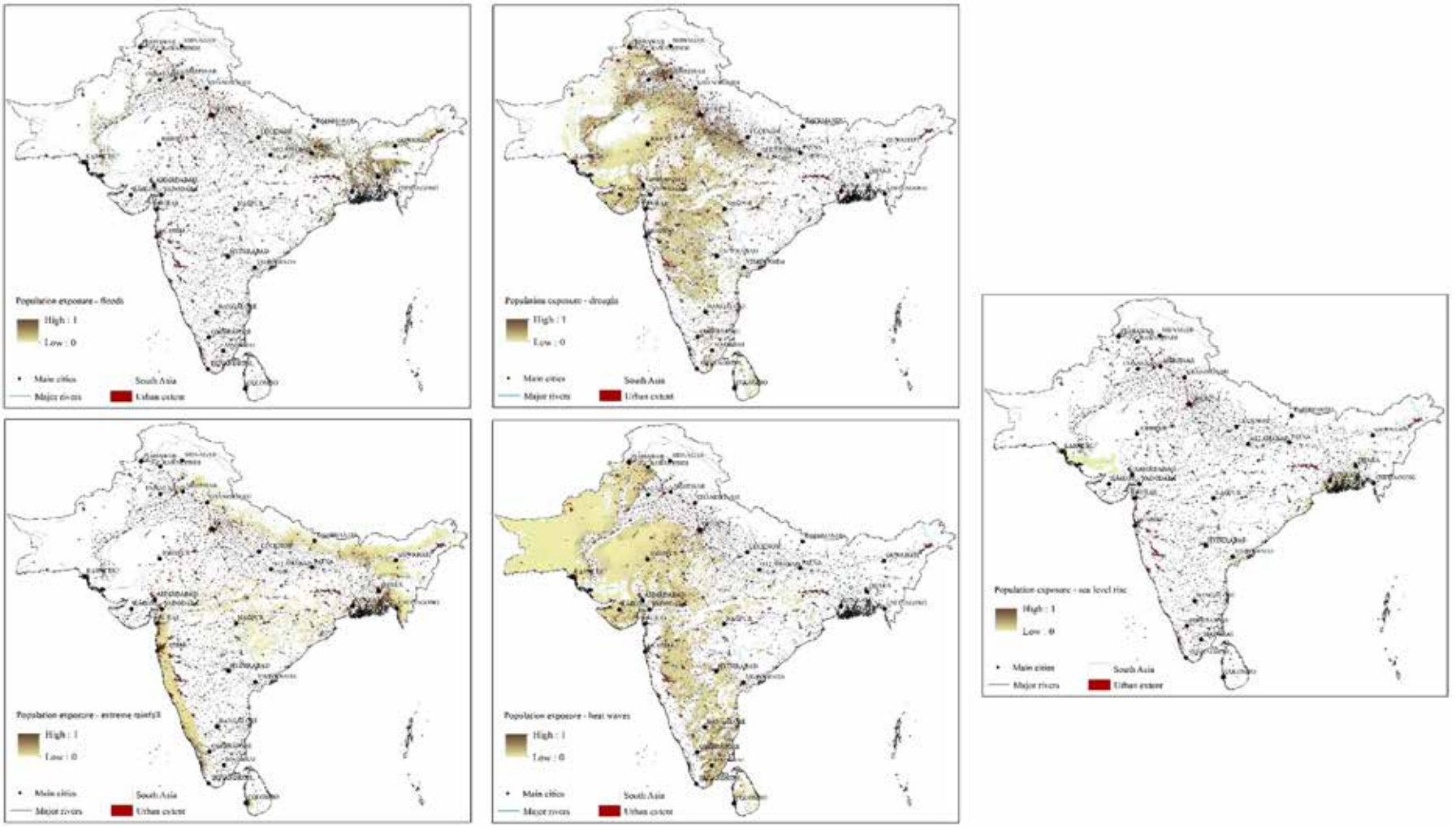

FIGURE 18. Population exposure to multiple climate hazards in eastern India and Bangladesh.

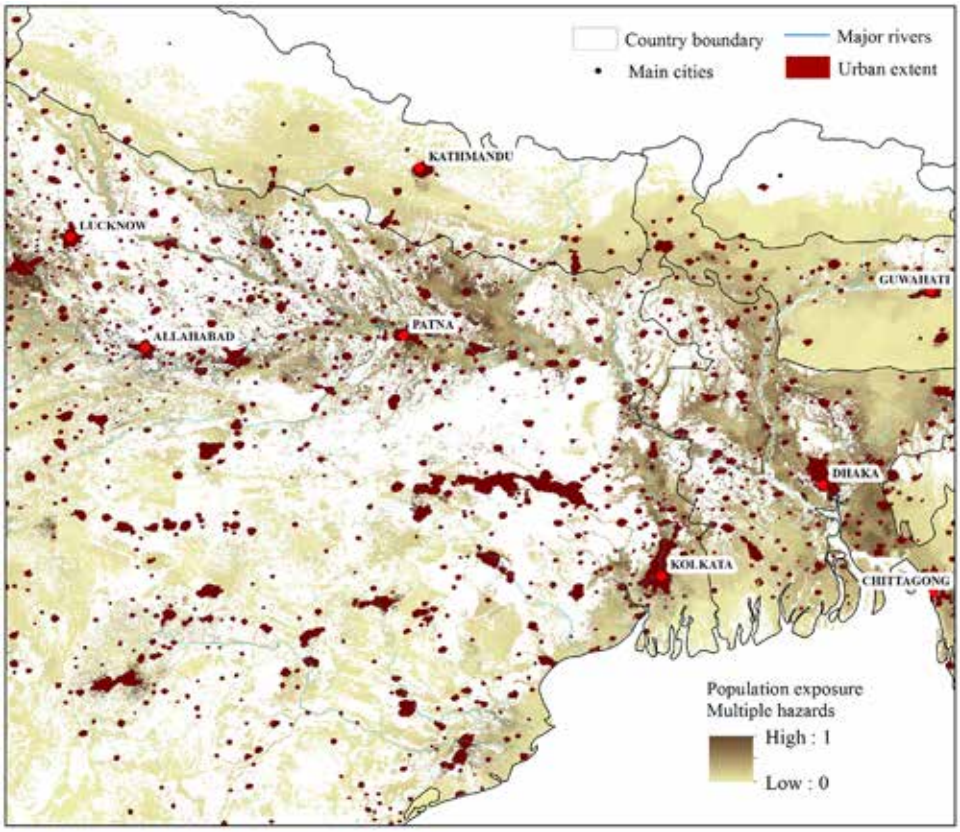

Note: The area of high exposure (dark brown overlaid with red urban extent) in Dhaka, Bangladesh, represents higher population exposure due to the dense concentration of people living in that area and is not necessarily higher population exposure. White areas in Dhaka represent locations where no climate hazard events were reported during the period of analysis.

Values of country/regional-level exposure to floods, droughts, extreme rainfall, heat waves and sea-level rise have a theoretical maximum value of 1 (i.e., the entire population of a country is exposed to the combined multiple hazard). Total average population exposure was calculated as the sum of exposure values of all cells in a country divided by the total population of all cells in the country (Equation [9]). The theoretical maximum value for total average population exposure is 5. Cell exposure values were calculated for each individual climate hazard (floods, droughts, extreme rainfall, heat waves and sea-level rise) and for multiple hazards together.

$$Average\ Population\ Exposure_{country} = \frac{\sum\ Cell\ Exposure_{country}}{Pop_{Total\ country}} \quad (9)$$

Country/regional scores were used to compare and rank countries/regions based on average population exposure to each individual climate hazard (floods, droughts, extreme rainfall, heat waves and sea-level rise) and for multiple hazards together.

Agricultural Exposure

Information on agricultural exposure to climate hazards was derived using SPOT vegetation land cover satellite data (Figure 19). Exposure was calculated separately for floods, droughts, extreme rainfall, heat waves and sea-level rise, as well as to estimate the overall damage from multiple climate hazards.

FIGURE 19. Land cover map used to quantify the impact of climate hazards on agriculture.

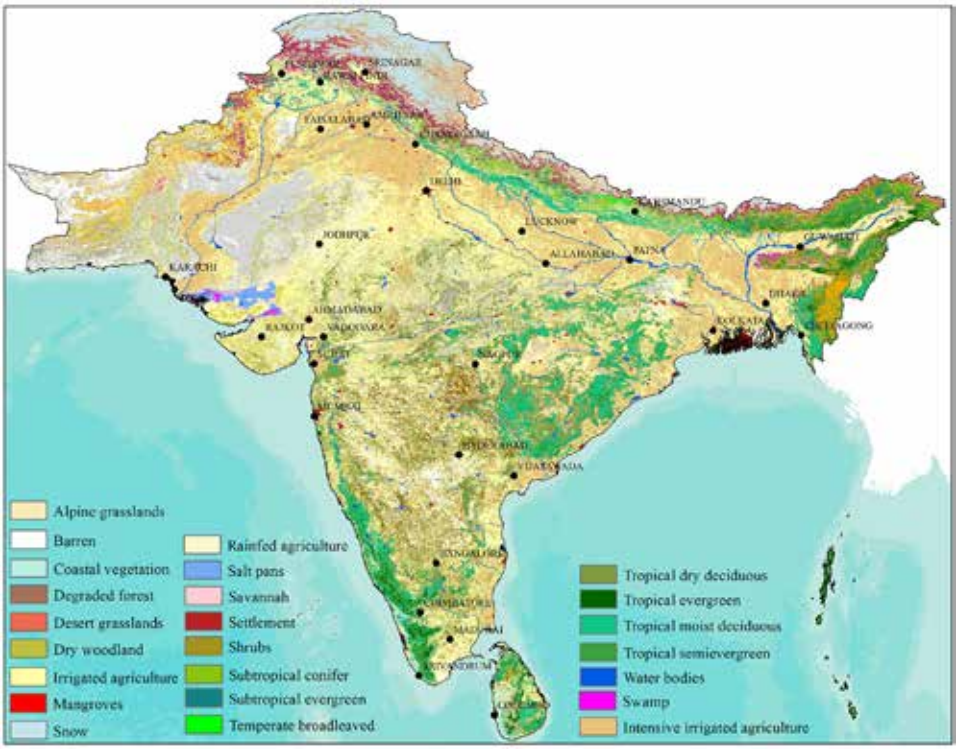

Data source: European Space Agency (ESA) Climate Change Initiative for South Asia.

Results and Discussion

Hazard-specific Impact Assessment

The overall climate hazard map (Figure 20) ranks district-level areas in South Asia according to their exposure to multiple hazards (floods, droughts, extreme rainfall, heat waves and sea-level rise). The darkest parts of the map indicate those areas that have the highest exposure to multiple hazards.

Results presented in this section are in the form of rankings based on integrated climate-hazard variables, and exposure related to agriculture and population at the sub-national and regional levels. In Figure 16, these are displayed as district-level exposure with equal intervals (maroon = highest quintile of exposed risk). Further, the multi-hazard ranks have been compared with sensitivity variables, including

population exposure, agricultural impacts and the Human Development Index (HDI), to identify areas vulnerable to risks (UNDP 2013, 2015). The 2012 HDI has been used in four development classes (low, medium, high and very high) based on the country's level of education, gross national income per capita and life expectancy at birth. For example, within South Asia, HDI values are higher for Bhutan, and selected states and provinces in Sri Lanka and India.

FIGURE 20. Classification of districts in South Asia according to their exposure to multiple hazards.

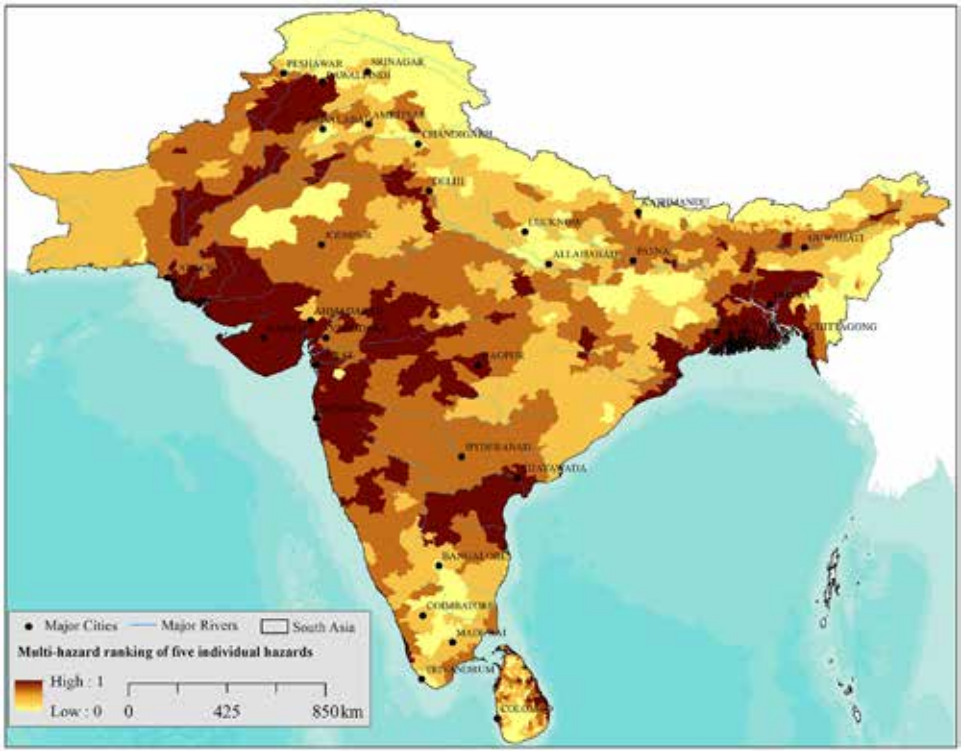

Population Exposure to Individual Hazards

Figures 17 and 18 describe population exposure to individual and multiple hazards, providing an interesting summary of exposure to the five climate-related hazards discussed in this report. Country-level rankings of population exposure to various hazards (floods and droughts, in particular) are listed in Tables 4 and 5. It can be seen that exposure to drought is more widespread than exposure to extreme rainfall and sea-level rise in South Asia. Populations with high exposure to drought during the 2001-2013 period of analysis include those in far northwestern India, Pakistan, and north and southeast Sri Lanka. Countries in South Asia that experience monsoon variability and a small decrease or delay in rainfall may be highly exposed to drought. Further, exposure to drought was greater as HDI class decreased. At the sub-national level, drought-prone states of Maharashtra, Gujarat and Rajasthan, with a low HDI value, may be highly vulnerable than the regions with medium HDI values in Sri Lanka.

Analyzing country-level population exposure revealed that approximately 750 million people are affected by climate hazards of some sort. Of the affected population, 72% come from India, followed by 12% each from Bangladesh and Pakistan. The remaining 4% is divided across Bhutan, Nepal and Sri Lanka. With regard to population exposure to individual hazards, droughts affect the most number of people (293 million). This is followed by extreme rainfall (220 million), floods (170 million), extreme temperature (76 million) and sea-level rise (59 million) (Table 5).

The population of nearly all South Asian countries, especially those living in the Indus, Ganges, Brahmaputra and Meghna river basins, was highly exposed to flooding during the 2000-2012 period of analysis. In contrast to drought, exposure to floods is distributed across all HDI classes. For example, Bangladesh, and the states of Bihar and Uttar Pradesh in India, along with Punjab and Sindh provinces in Pakistan, all with high population and low HDI values, are highly vulnerable areas. On the other hand, Bhutan and Sri Lanka, with moderate populations and high HDI values, are categorized as medium-risk areas.

Exposure to extreme rainfall is very similar to that of exposure to floods. Analysis of 65 years of rainfall data revealed that the frequency of extreme rainfall events is decreasing in major parts of central and north India, while they are increasing in peninsular, east and northeast India, and in the west of Sri Lanka. Nevertheless, extreme rainfall indices show increases in the South Asia average, consistent with globally averaged results (Kitoh et al. 2013). As with floods, population exposure to extreme rainfall is distributed across all HDI classes. For example, regions in east and northeast India, the Himalayas range in Nepal, and parts of Bangladesh, all with low HDI values, are highly vulnerable areas. Bhutan and Sri Lanka, with moderate populations and high HDI values, are, again, categorized as medium-risk areas.

TABLE 4. Population exposure corresponding to the number of occurrences of composite climate hazards.

Country	Population exposure to the total number of multiple hazards occurred				Total affected population (millions)	Total population (millions)
	1[a]	2[a]	3[a]	4[a] and 5[a]		
Bangladesh	59,436,143	28,496,623	3,476,050	38,957	91,447,774	156,600,000
Bhutan	227,261	104,235	373	0	331,869	743,224
India	402,789,651	129,692,215	6,559,698	224,376	539,265,941	1,252,000,000
Nepal	13,661,663	622,986	9,334	0	14,293,983	27,800,000
Pakistan	64,314,042	23,840,586	3,099,634	42,952	91,297,213	182,100,000
Sri Lanka	6,637,077	2,174,791	276,124	15,935	9,103,927	20,480,000

Note: [a] The frequency mentioned in this table refers to a number of occurrences of any type of climate hazard.

TABLE 5. Population exposure to individual hazards.

Country	Total affected population					Total affected population (millions)	Total population (millions)
	Floods	Droughts	Extreme rainfall	Extreme temperature	Sea-level rise		
Bangladesh	53,126,863	1,555,258	50,895,845	297,943	22,071,103	127.95	156.60
Bhutan	931	208,470	0	0	0	0.21	0.74
India	101,461,595	233,847,406	151,185,736	20,301,115	34,001,550	540.80	1,252.00
Nepal	1,590,753	614,902	12,713,208	225,243	0	15.14	27.80
Pakistan	13,753,696	54,940,373	948,089	50,925,713	2,709,392	123.28	182.10
Sri Lanka	1,045,301	2,046,134	4,304,666	4,712,980	660,238	12.77	20.48
Total	170,979,139	293,212,543	220,047,544	76,462,994	59,442,283		

In the case of heat waves, exposure is more broadly distributed than floods or extreme rainfall in South Asia. Populations with high exposure to heat waves during the 2001-2013 period of analysis include most parts of northwestern and southern India, Pakistan, and central and eastern Sri Lanka. At the sub-national level, states prone to heat waves in Andhra Pradesh, Telangana, Punjab, Uttar Pradesh, Odisha and Bihar in India, and Sindh, Punjab, Balochistan and Khyber Pakhtunkhwa provinces in Pakistan, with low HDI values, may be highly vulnerable when compared to regions with medium HDI values in Sri Lanka. The heat waves in India and Pakistan in 2015 killed more than 3,500 people, and was the deadliest such events since 1979. The heat waves were caused, in the large part, by sparser pre-monsoon seasonal showers, which brought less moisture than normal to the area. This left large parts of India and Pakistan dry. The cessation of pre-monsoon rain, an uncommon trend in India, contributed to the heat waves.

Exposure to sea-level rise was the highest in the states of West Bengal, Orissa and Maharashtra in India, followed by Bangladesh, Sindh in Pakistan, and Sri Lanka, during the period of analysis. Coastal regions with low HDI values are highly vulnerable to sea-level rise, followed by those with medium to high HDI values. Low-lying coastal cities are particularly vulnerable to the risks of storm surges and sea-level rise. These cities include Karachi, Mumbai, Chennai and Dhaka, all of which have witnessed significant environmental stresses in recent years. These cities are likely to become more vulnerable to flooding in the future because high seawater levels provide a higher base from which storm surges advance. Higher seawater levels will also potentially increase the risk of flooding due to rainstorms, by reducing coastal drainage. This is because sea-level rise also raises the local water table. All these effects have potentially devastating socioeconomic implications, particularly for infrastructure in low-lying, deltaic areas.

Impacts of Weather-related Hazards on Agriculture

Agriculture is particularly prone to multiple risks (Amendola et al. 2007; Christenson et al. 2014; Hirabayashi et al. 2013), including weather-related hazards, affecting many farmers at once. Some weather-related risks, such as droughts and floods, have a systemic component, in that they can affect most farmers within an entire region or country. Other weather-related risks, such as extreme rainfall and extreme temperature, are more location specific. Being exposed to such climate extremes, agriculture is an extremely vulnerable economic sector. The statistical analysis revealed that the dominant climate hazards affecting agricultural areas are droughts (786,000 km^2), followed by extreme temperature (651,000 km^2), extreme rainfall (218,000 km^2), floods (208,000 km^2) and sea-level rise (52,000 km^2) (Tables 6 and 7).

TABLE 6. Agricultural impacts due to different frequencies of combined hazards.

Country	Agricultural areas affected as a result of the toztal number of multiple hazards occurred (km^2)				Affected area	Agriculture (km^2)*
	1[a]	2[a]	3[a]	4[a] and 5[a]		
Bangladesh	46,403.5	24,035.5	3,226.7	20.7	73,686.5	91,280
Bhutan	1,008.5	5	0	0	1,013.5	5,196
India	654,288.7	363,231.5	10,754	502.5	1,028,777	1,796,700
Nepal	21,698.7	631.7	11.5	0	22,342	41,266
Pakistan	123,990.7	82,237.5	14,119	358.7	220,706	359,360
Sri Lanka	7,308.2	4,361.5	268	8.2	11,946	27,300

Notes: [a] The frequency mentioned in this table refers to the number of occurrences of any type of climate hazard.

[*] Data from the statistical online database of the Food and Agriculture Organization of the United Nations (FAO).

At the country level, agricultural losses as a result of individual climate hazards are highest in India, followed by Pakistan, Bangladesh, Nepal, Sri Lanka and Bhutan. With regard to agricultural losses in India, drought has had the most widespread impact (affecting 594,000 km^2), followed by extreme temperature (523,000 km^2), extreme rainfall (155,000 km^2), floods (126,000 km^2) and sea-level rise (30,000 km^2) (Table 7).

TABLE 7. Impact of individual hazards on agriculture.

Country	Agricultural areas affected due to different types of climate hazard (km^2)					
	Floods	Droughts	Extreme rainfall	Extreme temperature	Sea-level rise	Agriculture (km^2)*
Bangladesh	48,471.20	2,666.80	38,902.10	1,643.40	16,794.40	91,280
Bhutan	8.1	4.5	1,038.60	0	0	5,196
India	126,153.10	594,805.50	155,932.80	523,268	30,203.90	1,796,700
Nepal	2,456.50	1,093.60	21,049.20	143.3	0	41,266
Pakistan	30,015.30	181,265.40	1,055.90	118,847.90	4,893.30	359,360
Sri Lanka	1,171.90	6,828.40	972.3	7,376.50	571.2	27,300
Total	208,276.10	786,664.20	218,950.90	651,279.10	52,462.80	

Notes: * Data from the statistical online database of FAO.

Overall Climate Change Vulnerability Map

To obtain the overall index of climate change vulnerability, we normalized each of the indicators of exposure (multiple hazard risks), sensitivity (human population and agriculture) and adaptive capacity (HDI). To identify the vulnerable areas, we ranked the regions according to the HDI and divided the list into three grouped datasets. Those states/districts falling in the fourth quartile were considered the vulnerable areas and further classified as low to high vulnerability areas. We used two different methods of ranking the areas: (i) across the whole of South Asia, and (ii) within each of the individual countries. This was done simply to rank priority areas for adaptation interventions by different users of this mapping information. Figure 20 shows the district map of multi-hazard areas in South Asia as a function of agricultural and population exposure.

Using the method outlined above to derive a climate change vulnerability map, we identified the most vulnerable areas in South Asia (Figure 21). The areas with high quartile include most regions of Bangladesh, northwestern India, north and east of Pakistan, and regions to the west and east of Sri Lanka (Table 8). Unlike other countries in South Asia, India is not only exposed to floods (particularly in the Ganges River Basin and western parts of the country) and droughts, but is also exposed to many other climate-related hazards, including extreme temperature (northwestern and south India), extreme rainfall (Northeast, Western Ghats and Central India) and sea-level rise. Table 8 lists the climate-hazard hot spots and the dominant hazards likely to affect these areas.

Figure 21 shows the most vulnerable regions within countries, i.e., those in the top quartile relative to other areas within each country. The availability of HDI data varies across South Asia. HDI information at district level is only available for Bhutan and Sri Lanka. Therefore, current risk analysis is limited to subregional level. Using a scatter plot (Figure 22), with the datasets described above, four categories (low, medium, high and extreme risk) were identified (Table 9). Using the ranking procedure, we found that most of the divisions in Bangladesh; the Indian states of Andhra Pradesh, Bihar, Maharashtra, Karnataka and Orissa; Ampara, Puttalam, Trincomalee, Mannar and Batticaloa in Sri Lanka; Sindh and Balochistan in Pakistan; and Central and East Nepal are extreme-risk areas. The low-risk areas are regions in Bhutan, because there are fewer climate hazards and those that occur have minimal impact on population and agriculture due to high HDI values.

FIGURE 21. Climate change vulnerability map of South Asia based on exposure, sensitivity and adaptive capacity to multiple hazards.

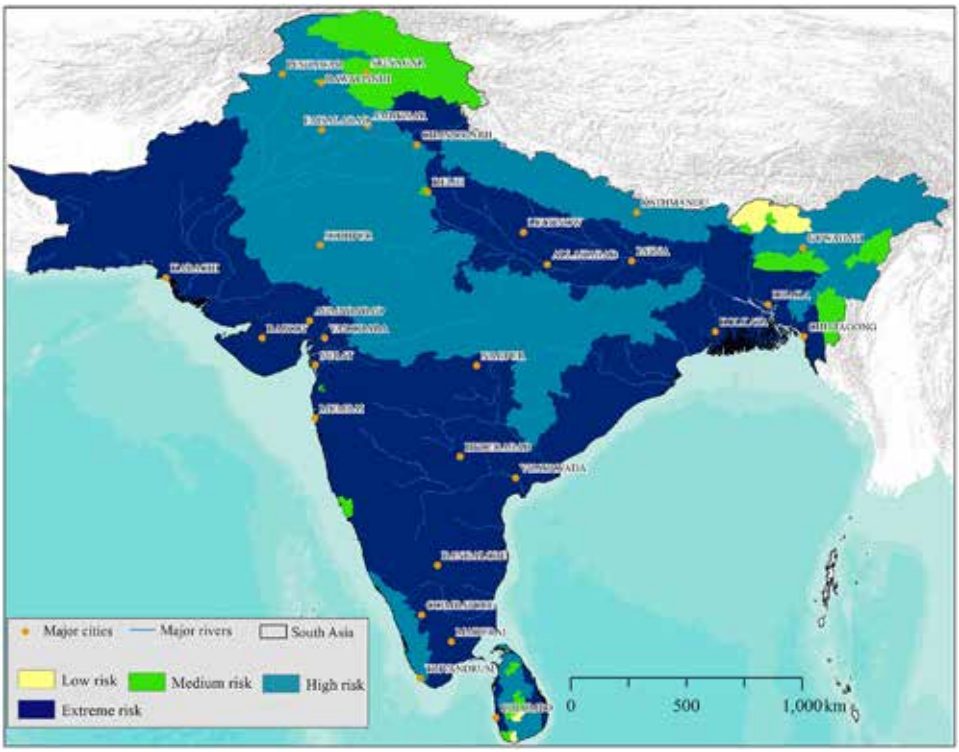

TABLE 8. The climate-hazard hot spots and the dominant hazards likely to affect these areas.

Climate-hazard hot spots	Dominant hazards
Northwestern India	Droughts and heat waves
Eastern coastal areas of India	Sea-level rise, floods
Northeastern region	Extreme rainfall and floods
Bangladesh	Floods, sea-level rise, extreme rainfall, droughts
Pakistan	Floods, droughts, heat waves
Central India	Droughts, heat waves, extreme rainfall
Western and eastern area of Sri Lanka	Floods, droughts, sea-level rise, extreme rainfall
Terai region of Nepal	Floods, droughts and extreme rainfall

In general, the results provide no surprises, as they confirm commonly held suspicions that the most vulnerable regions of South Asia include the coastal region of Bangladesh, the Indian states of West Bengal, Orissa, Andhra Pradesh and Gujarat, and Sindh in Pakistan. The vulnerability of these regions is linked to their exposure to sea-level rise, and their positions in relation to the transboundary river basins of the Ganges, Brahmaputra and Meghna (GBM), which are prone to annual flooding. It is surprising to see that most regions of Bhutan, by comparison, are not fully exposed to climate hazards; however, their low level of vulnerability reflects their high adaptive capacity (high HDI values). Exceptions are the districts of Geylegphug, Samchi and Chhukha, which suffer from flooding and extreme rainfall.

FIGURE 22. Scatter plot illustrating the hazard-risk areas derived using composite variables, including exposure (hazard risks), sensitivity (human population and agriculture) and adaptive capacity (HDI values).

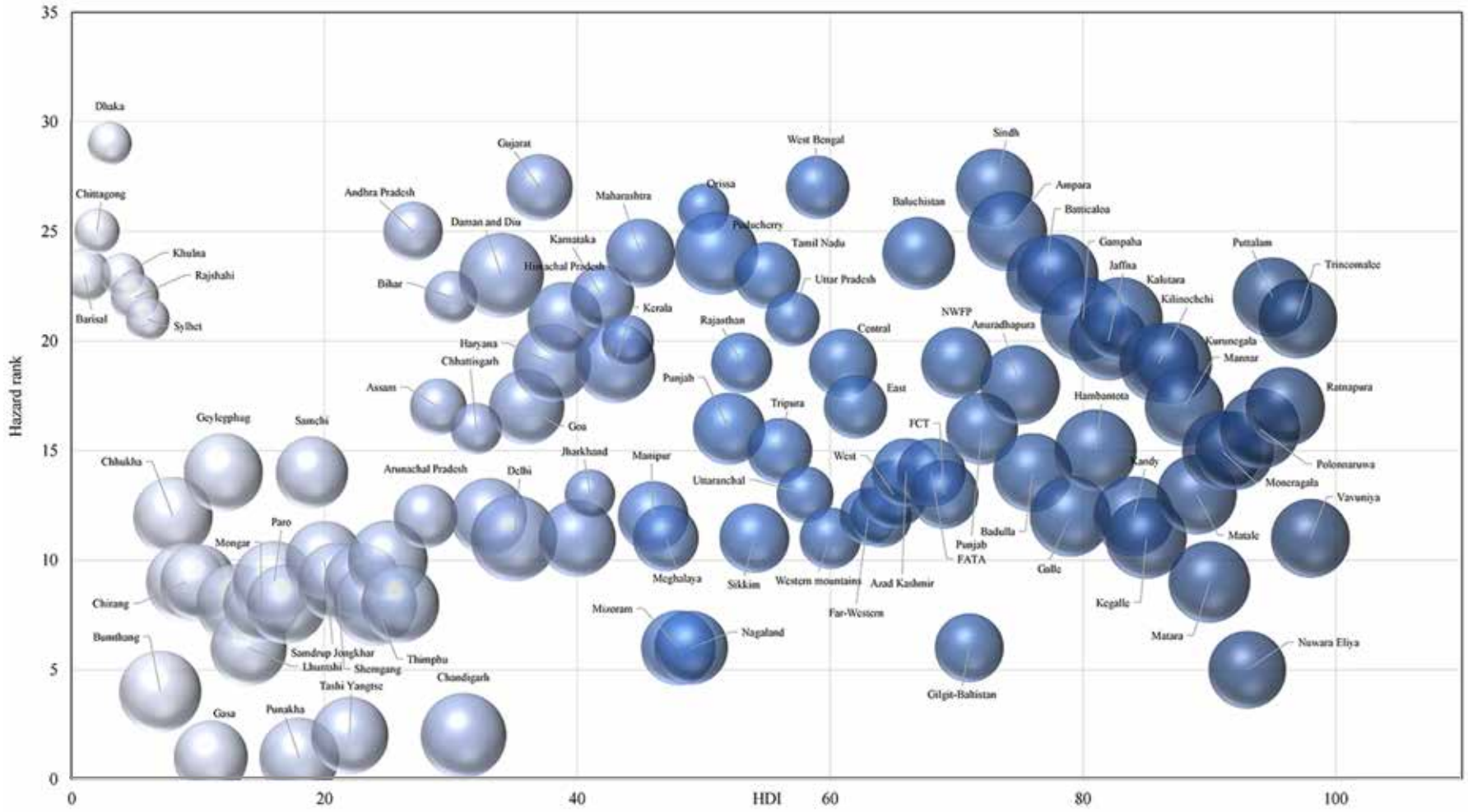

Notes: The light to dark blue coloring represents low to high values, with the names identifying administrative units across South Asia.

FATA = Federally Administered Tribal Areas; FCT = Federal Capital Territory; NWFP = North-West Frontier Province or Khyber Pakhtunkhwa.

TABLE 9. Three parameters (hazard, exposure and adaptive capacity) are used to rank low- to extreme-risks areas for South Asia.

Risk/Parameters	Low	Medium	High	Extreme
Hazards (floods, droughts, extreme rainfall, heat waves, sea-level rise)	Low	Moderate	High	Very high
Exposure (population exposure and agricultural losses)				
Adaptive capacity (Human Development Index)	High	Moderate	Low	Very low
Countries/States	Bhutan; Sri Lanka: districts of Nuwara Eliya and Matara	Bhutan: Geylegphug, Samchi and Chhukha; India: Meghalaya, Nagalard, Mizoram, Jammu and Kashmir; Pakistan: Gilgit-Baltistan; Sri Lanka: Kandy, Badulla and Kegalle	India: Rajasthan, Madhya Pradesh, Chhattisgarh, Jharkhand, Assam, Punjab and Haryana; Pakistan: Punjab, Khyber Pakhtunkhwa, FATA; Sri Lanka: Anuradhapura, Kurunegala and Polonnaruwa; Nepal: West, Far-western, Mid-western, Western Mountains	Most of Bangladesh; India: Andhra Pradesh, Bihar, Maharashtra, Karnataka and Orissa; Sri Lanka: Ampara, Puttalam, Trincomalee, Mannar and Batticaloa; Pakistan: Sindh and Balochistan; Central and East Nepal

Adaptive capacity seems to have a large influence on the spatial pattern of vulnerability. The low adaptive capacity of Bangladesh means it has some of the most vulnerable regions that are highly exposed to climate hazards. On the other hand, the high adaptive capacity of the North, North-central, Central, Uva and Southern provinces in Sri Lanka, which are susceptible to droughts, floods and extreme temperature, has enabled these areas to moderate their vulnerability. As a result, they are not included among the most vulnerable areas of South Asia. However, this does not apply as a general rule, as there are other areas where high adaptive capacity does not help to moderate exposure to climate risks. Mumbai, Dhaka, Kolkata and Karachi are good examples of regions that are highly affected by frequent floods in spite of their high adaptive capacity. This is because the adaptive capacities of those cities are not sufficient to moderate their extreme vulnerability, which is brought about by their high population densities and significant exposure to climate hazards (in particular, floods and sea-level rise). The current study has not included other hazards, such as landslides, to which many of these provinces are also highly vulnerable. Glacial lake outburst floods, cyclones, wildfires and other hazards have also been excluded from this study; including them would result in changes to vulnerability patterns.

Conclusions

This study presents a detailed and coherent approach to mapping climate hazards and identifying risk areas in South Asia, which, for the first time, combines the following unique features: (a) consistent methodology across the study of different climate-related hazards, (b) assessment

of total population affected and agricultural losses, (c) regional-level spatial coverage, and (d) application of customized tools using the ArcGIS toolbox. This toolbox facilitates the assessment of changes in exposure to hazards over time, and can be easily updated when a newly released or superior dataset becomes available. This enables comparison of climate-related hazards among the most vulnerable regions in South Asia, which can be considered to have the most urgent policy needs.

The methodology and analysis introduced in this paper enabled us to estimate exposure to a range of climate-related hazard events, including floods, droughts, extreme rainfall, extreme temperature and sea-level rise. A multi-hazard parameter was devised to sum up the total exposure to these five hazard events, with a focus on population exposure (the relative hazard frequency in a given area weighted by population count). This approach enables population exposure to be calculated for diverse climate-related outcomes (e.g., mortality due to hazards, as previous studies have done, or population at risk from loss of drinking water or agricultural productivity). Further, the hazard and exposure were compared across countries against HDI classes. Exposure to floods and droughts were highest in countries with a high HDI value; they also disproportionately affected countries with low and medium HDI values. Exposure to sea-level rise was highest in countries with a high HDI, whereas exposure to droughts was highest in those with a low HDI, mainly in India and Pakistan.

We gathered a wide range of remote sensing data and products, as well as socioeconomic data at provincial and district levels, from various sources, and integrated these details in a consistent and meaningful manner to produce a map indicating the areas most vulnerable to climate change. This assessment of exposure to climate hazards has implications for country-level adaptation to climate change. It could be used to help inform decisions about financial aid or how to allocate adaptation resources within a country, for example. Additionally, the assessment allows comparisons to be made between different countries' exposure to a particular hazard. The model is designed to be flexible, allowing exposure assessment methods to be applied to a range of outcomes and adaptation measures, such as mortality, economic loss, costs of repair to water infrastructure, sanitation risks, or other outcomes that may occur due to the climate-related hazards outlined.

References

Abid, M.; Schilling, J.; Scheffran, J.; Zulfiqar, F. 2016. Climate change vulnerability, adaptation and risk perceptions at farm level in Punjab, Pakistan. *Science of the Total Environment* 547: 447-460.

ADPC (Asian Disaster Preparedness Center). 2010. *Nepal hazard risk assessment*. Asian Disaster Preparedness Centre (ADPC); Norwegian Geotechnical Institute (NGI); Centre for International Studies and Cooperation (CECI). 237p.

Amarnath, G. 2014a. An algorithm for rapid flood inundation mapping from optical data using a reflectance differencing technique. *Journal of Flood Risk Management* 7(3): 239-250.

Amarnath, G. 2014b. Earth observation data: Monitoring floods and drought. *Geospatial Today* 6: 15-19.

Amarnath, G.; Ameer, M.; Aggarwal, P.; Smakhtin, V. 2012. Detecting spatio-temporal changes in the extent of seasonal and annual flooding in South Asia using multi-resolution satellite data. In: *Earth resources and environmental remote sensing/GIS applications III: Proceedings of the International Society for Optics and Photonics (SPIE), Vol. 8538, Amsterdam, Netherlands, July 1-6, 2012*. Bellingham, WA, USA: International Society for Optics and Photonics (SPIE). 11p.

Amarnath, G.; Clarke, J. 2016. Drought monitoring system helps strengthen resiliency to climate change. *World Water* 39(1): 14-15.

Amendola, A.; Linnerooth-Bayer, J.; Okada, N.; Shi, P. 2007. Towards integrated disaster risk management: Case studies and trends from Asia. *Natural Hazards* 44: 163-168.

Badas, M.G.; Deidda, R.; Piga, E. 2005. Orographic influences in rainfall downscaling. *Advances in Geosciences* 2: 285-292.

Bhuiyan, C.; Singh, R.P.; Kogan, F.N. 2006. Monitoring drought dynamics in the Aravalli region (India) using different indices based on ground and remote sensing data. International Journal of Applied Earth Observation and Geoinformation 8(4): 289-302.

Brown, J.F.; Wardlow, B.D.; Tadesse, T.; Hayes, M.J.; Reed, B.C. 2008. The Vegetation Drought Response Index (VegDRI): A new integrated approach for monitoring drought stress in vegetation. *GIScience and Remote Sensing* 45(1): 16-46.

Christenson, E.; Elliott, M.; Banerjee, O.; Hamrick, L.; Bartram, J. 2014. Climate-related hazards: A method for global assessment of urban and rural population exposure to cyclones, droughts, and floods. *International Journal of Environmental Research and Public Health* 11(2): 2169-2192.

CIESIN (Center for International Earth Science Information Network); Columbia University; CIAT (Centro Internacional de Agricultura Tropical). 2005a. *Gridded Population of the World, Version 3 (GPWv3): Population density grid*. Palisades, NY, USA: NASA Socioeconomic Data and Applications Center (SEDAC). Available at http://sedac.ciesin.columbia.edu/data/set/ gpw-v3-population-density (accessed on August 30, 2014).

CIESIN (Center for International Earth Science Information Network); Columbia University; Food and Agriculture Organization of the United Nations (FAO); CIAT (Centro Internacional de Agricultura Tropical). 2005b. *Gridded Population of the World, Version 3 (GPWv3): Population count grid*. Palisades, NY, USA: NASA Socioeconomic Data and Applications Center (SEDAC). Available at http://dx.doi.org/10.7927/H4639MPP (accessed on July 21, 2015).

Cleve, C.; Kelly, M.; Kearns, F.R.; Moritz, M. 2008. Classification of the wildland–urban interface: A comparison of pixel- and object-based classifications using high-resolution aerial photography. *Computers, Environment and Urban Systems* 32(4): 317-326.

Cutter, S.L.; Finch, C. 2008. Temporal and spatial changes in social vulnerability to natural hazards. *Proceedings of the National Academy of Sciences of the United States of America* 105(7): 2301-2306.

Deen, S. 2015. Pakistan 2010 floods. Policy gaps in disaster preparedness and response. *International Journal of Disaster Risk Reduction* 12: 341-349.

Dilley, M.; Chen, R.S.; Deichmann, U.; Lerner-Lam, A.L.; Arnold, M.; Agwe, J.; Buys, P.; Kjekstad, O.; Lyon, B.; Yetman, G. 2005. *Natural disaster hotspots: A global risk analysis*. Washington, DC, USA: International Bank for Reconstruction and Development/The World Bank, and Columbia University.

Dotsenko, S.F. 2005. Run-up of a solitary tsunami wave on a sloping coast. *Journal of Physical Oceanography* 15(4): 211-219.

Dutta, D.; Kundu, A.; Patel, N.R. 2013. Predicting agricultural drought in eastern Rajasthan of India using NDVI and standardized precipitation index. *Geocarto International* 28: 192-209.

EM-DAT. 2015. The OFDA/CRED international disaster database [Internet]. Brussels: Universit_e catholique de Louvain. Available at http://www.emdat.net (accessed January 27, 2015).

Füssel, H-M.; Klein, R.J.T. 2006. Climate change vulnerability assessments: An evolution of conceptual thinking. *Climatic Change* 75(3): 301-329.

Gallina, V.; Torresan, S.; Critto, A.; Sperotto, A.; Glade, T.; Marcomini, A. 2016. A review of multi-risk methodologies for natural hazards: Consequences and challenges for a climate change impact assessment. *Journal of Environmental Management* 168: 123-132.

Gebrehiwot, T.; van der Veen, A.; Maathuis, B. 2011. Spatial and temporal assessment of drought in the Northern highlands of Ethiopia. *International Journal of Applied Earth Observation and Geoinformation* 13(3): 309-321.

Ghulam, A.; Li, Z.L.; Qin, Q.; Tong, Q. 2007. Exploration of the spectral space based on vegetation index and albedo for surface drought estimation. *Journal of Applied Remote Sensing* 1(013529): 1-12.

Gouveia, C.M.; Bastos, A.; Trigo, R.M.; DaCamara, C.C. 2012. Drought impacts on vegetation in the pre- and post-fire events over Iberian peninsula. *Natural Hazards and Earth System Sciences* 12(10): 3123-3137.

Gu, Y.; Brown, J.F.; Verdin, J.P.; Wardlow, B. 2007. A five-year analysis of MODIS NDVI and NDWI for grassland drought assessment over the central Great Plains of the United States. *Geophysical Research Letters* 34(6).

Guha-Sapir, D.; Vos, F.; Below, R.; Ponserre, S. 2012. *Annual disaster statistical review 2011: The numbers and trends*. Brussels: Centre for Research on the Epidemiology of Disasters (CRED).

Guhathakurta, P.; Rajeevan, M. 2006. *Trends in the rainfall pattern over India*. NCC Research Report 2. Pune, India: National Climate Centre (NCC), India Meteorological Department.

Guleria, S.; Patterson Edward, J.K. 2012. Coastal community resilience: Analysis of resilient elements in 3 districts of Tamil Nadu State, India. *Journal of Coastal Conservation* 16(1): 101-110.

Gupta, A.K.; Tyagi, P.; Sehgal, V.K. 2011. Drought disaster challenges and mitigation in India: Strategic appraisal. *Current Science* 100(12): 1795-1806.

Hirabayashi, Y.; Mahendran, R.; Koirala, S.; Konoshima, L.; Yamazaki, D.; Watanabe, S.; Kim, H.; Kanae, S. 2013. Global flood risk under climate change. *Nature Climate Change* 3: 816-821.

Immerzeel, W.W.; Rutten, M.M.; Droogers, P. 2009. Spatial downscaling of TRMM precipitation using vegetative response on the Iberian peninsula. *Remote Sensing of Environment* 113(2): 362-370.

IPCC (Intergovernmental Panel on Climate Change). 2012. Summary for policymakers. In: *Managing the risks of extreme events and disasters to advance climate change adaptation*, eds., Field, C.B.; Barros, V.; Stocker, T.F.; Qin, D.; Dokken, D.J.; Ebi, K.L.; Mastrandrea, M.D.; Mach, K.J.; Plattner, G.-K.; Allen, S.K.; Tignor, M.; Midgley, P.M. A Special Report of Working Groups I and II of the Intergovernmental Panel on Climate Change. Cambridge University Press, Cambridge, UK, and New York, NY, USA. Pp. 1-19.

IPCC (Intergovernmental Panel on Climate Change). 2014. *Climate change 2014: Impacts, adaptation, and vulnerability. Part B: Regional aspects. Contribution of Working Group II to the Fifth Assessment Report of the Intergovernmental Panel on Climate Change*, eds., Barros, V.R.; Field, C.B.; Dokken, D.J.; Mastrandrea, M.D.; Mach, K.J.; Bilir, T.E.; Chatterjee, M.; Ebi, K.L.; Estrada, Y.O.; Genova, R.C.; Girma, B.; Kissel, E.S.; Levy, A.N.; MacCracken, S.; Mastrandrea, P.R.; White, L.L. Cambridge, United Kingdom, and New York, NY, USA: Cambridge University Press. 688p.

Jain, S.K.; Saraf, A.K.; Goswami, A.; Ahmad, T. 2006. Flood inundation mapping using NOAA AVHRR data. *Water Resources Management* 20(6): 949-959.

Jensen, J.R. 2005. *An introductory digital image processing: A remote sensing perspective*. Upper Saddle River, NJ: Prentice Hall. 526p.

Kappes, M.S.; Papathoma-Köhle, M.; Keiler, M. 2012a. Assessing physical vulnerability for multi-hazards using an indicator-based methodology. *Applied Geography* 32(2): 577-590.

Kappes, M.S.; Keiler, M.; von Elverfeldt, K.; Glade, T. 2012b. Challenges of analyzing multi-hazard risk: A review. *Natural Hazards* 64(2): 1925-1958.

Karim, M.F.; Mimura, N. 2008. Impacts of climate change and sea-level rise on cyclonic storm surge floods in Bangladesh. *Global Environmental Change* 18(3): 490-500.

Kitoh, A.; Endo, H.; Krishna Kumar, K.; Cavalcanti, I.F.A.; Goswami, P.; Zhou, T. 2013. Monsoons in a changing world: A regional perspective in a global context. *Journal of Geophysical Research: Atmospheres* 118: 3053-3065.

Kogan, F.N. 1995. Application of vegetation index and brightness temperature for drought detection. *Advances in Space Research* 15(11): 91-100.

Kundzewicz, Z.W.; Hirabayashi, Y.; Kanae, S. 2009. River floods in the changing climate – observations and projections. *Water Resources Management* 24: 2633-2646.

Kunte, P.D.; Jauhari, N.; Mehrotra, U.; Kotha, M.; Hursthouse, A.S.; Gagnon, A.S. 2014. Multi-hazards coastal vulnerability assessment of Goa, India, using geospatial techniques. *Ocean and Coastal Management* 95: 264-281.

Lerner-Lam, A. 2007. Assessing global exposure to natural hazards: Progress and future trends. *Environmental Hazards* 7(1): 10-19.

Liu, C.; Wu, J. 2008. Crop drought monitoring using MODIS NDDI over mid-territory of China. In: *Proceedings of the 2008 IEEE International Geoscience and Remote Sensing Symposium: Volume 3, July 7-11, 2008, Boston, Massachusetts, USA*. Pp. 883-886.

Malone, E.L.; Engle, N.L. 2011. Evaluating regional vulnerability to climate change: Purposes and methods. *Wiley Interdisciplinary Reviews: Climate Change* 2(3): 462-474.

Mani Murali, R.; Ankita, M.; Amrita, S.; Vethamony, P. 2013a. Coastal vulnerability assessment of Puducherry coast, India, using the analytical hierarchical process. *Natural Hazards and Earth System Sciences* 13(12): 3291-3311.

MoDM (Ministry of Disaster Management). 2005. *Towards a safer Sri Lanka: Road map for disaster risk management*. Colombo, Sri Lanka: Disaster Management Centre, Ministry of Disaster Management, Government of Sri Lanka. Available at http://www.preventionweb.net/files/17954_goslroadmapdismanagcentre.pdf (accessed on September 23, 2015).

Mishra, A.K.; Singh, V.P. 2009. A review of drought concepts. *Journal of Hydrology* 391(1-2): 202-216.

Mosquera-Machado, S.; Dilley, M. 2009. A comparison of selected global disaster risk assessment results. *Natural Hazards* 48(3): 439-456.

Murari, K.K.; Ghosh, S.; Patwardhan, A.; Daly, E.; Salvi, K. 2015. Intensification of future severe heat waves in India and their effect on heat stress and mortality. *Regional Environmental Change* 15(4): 569-579.

Onema, J.-M.K.; Taigbenu, A. 2009. NDVI–rainfall relationship in the Semliki watershed of the equatorial Nile. *Physics and Chemistry of the Earth, Parts A/B/C* 34(13-16): 711-721.

Orencio, P.M.; Fujii, M. 2014. A spatiotemporal approach for determining disaster-risk potential based on damage consequences of multiple hazard events. *Journal of Risk Research* 17(7): 815-836.

Pasini, S.; Torresan, S.; Rizzi, J.; Zabeo, A.; Critto, A.; Marcomini, A. 2012. Climate change impact assessment in Veneto and Friuli Plain groundwater. Part II: A spatially resolved regional risk assessment. *Science of the Total Environment* 440: 219-235.

Patel, N.R.; Chopra, P.; Dadhwal, V.K. 2007. Analyzing spatial patterns of meteorological drought using standardized precipitation index. *Meteorological Applications* 14(4): 329-336.

Patel, N.R.; Parida, B.R.; Venus, V.; Saha, S.K.; Dadhwal, V.K. 2012. Analysis of agricultural drought using vegetation temperature condition index (VTCI) from Terra/MODIS satellite data. *Environmental Monitoring and Assessment* 184(12): 7153-7163.

Pattanaik, D.R.; Rajeevan, M. 2010. Variability of extreme rainfall events over India during southwest monsoon season. *Meteorological Applications* 17(1): 88-104.

Rafiq, L.; Blaschke, T. 2012. Disaster risk and vulnerability in Pakistan at a district level. *Geomatics, Natural Hazards and Risk* 3(4): 324-341.

Qin, Q.; Ghulam, A.; Zhu, L.; Wang, L.; Li, J.; Nan, P. 2008. Evaluation of MODIS derived perpendicular drought index for estimation of surface dryness over northwestern China. *International Journal of Remote Sensing* 29(7): 1983-1995.

Rhee, J.; Im, J.; Carbone, G.J. 2010. Monitoring agricultural drought for arid and humid regions using multi-sensor remote sensing data. *Remote Sensing of Environment* 114(12): 2875-2887.

Rufat, S.; Tate, E.; Burton, C.G.; Maroof, A.S. 2015. Social vulnerability to floods: Review of case studies and implications for measurement. *International Journal of Disaster Risk Reduction* 14(Part 4): 470-486.

Sakamoto, T.; Nguyen, N.V.; Kotera, A.; Ohno, H.; Ishitsuka, N.; Yokozawa, M. 2007. Detecting temporal changes in the extent of annual flooding within the Cambodia and the Vietnamese Mekong Delta from MODIS time-series imagery. *Remote Sensing of Environment* 109(3): 295-313.

Salik, K.M.; Jahangir, S.; Zahdi, W.Z.; Hasson, S. 2015. Climate change vulnerability and adaptation options for the coastal communities of Pakistan. *Ocean and Coastal Management* 112: 61-73.

Saxena, S.; Purvaja, R.; Mary Divya Suganya, D.; Ramesh, R. 2013. Coastal hazard mapping in the Cuddalore region, South India. *Natural Hazards* 66(3): 1519-1536.

Scolobig, A.; Garcia-Aristizabal, A.; Komendatova, N.; Patt, A.; Di Ruocco, A; Gasparini, P.; Monfort, D.; Vinchon, C.; Bengoubou-Valerius, M.; Mrzyglocki, R.; Fleming, K. 2014. From multi-risk assessment to multi-risk governance: Recommendations for future directions. In: *Understanding risk: The evolution of disaster risk assessment*. Washington, DC: International Bank for Reconstruction and Development/International Development Association or The World Bank. Pp. 163-167.

SDMC (South Asian Association for Regional Cooperation [SAARC] Disaster Management Centre). 2010. SAARC Workshop on Drought Risk Management in South Asia, August 8-9, 2010, Kabul, Afghanistan. New Delhi, India: SAARC Disaster Management Centre (SDMC). 183p.

Sharma, C.S.; Behera, M.D.; Panda, S.N.; Panda, S.N. 2011. Assessing flood induced land-cover changes using remote sensing and fuzzy approach in Eastern Gujarat (India). *Water Resources Management* 25: 3219-3246.

Srinivasa Kumar, T.; Mahendra, R.S.; Nayak, S.; Radhakrishnan, K.; Sahu, K.C. 2010. Coastal vulnerability assessment for Orissa State, East Coast of India. *Journal of Coastal Research* 26(3): 523-534.

Sterr, H.; Klein, R.J.T.; Reese, S. 2000. Climate change and coastal zones: An overview of the state-of-the-art on regional and local vulnerability. In: *Climate change in the Mediterranean: Socio-economic perspective of impacts, vulnerability and adaptation*, eds., Giupponi, C.; Shechter, M. Camberley, UK: Edward Elgar Publishing. Pp. 245-278.

Thenkabail, P.S.; Gamage, M.S.D.N.; Smakhtin, V. 2004. *The use of remote sensing data for drought assessment and monitoring in Southwest Asia*. Colombo, Sri Lanka: International Water Management Institute (IWMI). 30p. (IWMI Research Report 85).

Thieler, E.R. 2000. *National assessment of coastal vulnerability to future sea-level rise*. USGS Fact Sheet, fs-076-100.

UNDP (United Nations Development Programme). 2013. *Human development report 2013: The rise of the South: Human progress in a diverse world*. New York, USA: United Nations Development Programme (UNDP).

UNDP. 2015. *Human development report 2015: Work for human development*. New York, USA: United Nations Development Programme (UNDP).

UNISDR (United Nations International Strategy for Disaster Reduction). 2009. *Global assessment report on disaster risk reduction*. Technical Report. Geneva, Switzerland: United Nations International Strategy for Disaster Reduction (UNISDR).

Wan, Z.; Dozier, J. 1996. A generalized split-window algorithm for retrieving landsurface temperature from space. *IEEE Transactions on Geoscience and Remote Sensing* 34(4): 892-905.

Wan, Z. 2008. New refinements and validation of the MODIS land-surface temperature/emissivity products. *Remote Sensing of Environment* 112(1): 59-74.

Wan, Z. 2014. New refinements and validation of the collection-6 MODIS land-surface temperature/emissivity product. *Remote Sensing of Environment* 140: 36-45.

Weng, Q.; Lu, D.; Schubring, J. 2004. Estimation of land surface temperature–vegetation abundance relationship for urban heat island studies. *Remote Sensing of Environment* 89(4): 467-483.

Xiao, X.; Boles, S.; Liu, J.; Zhuang, D.; Frolking, S.; Li, C.; Salas, W.; Moore, B. 2005. Mapping paddy rice agriculture in southern China using multi-temporal MODIS images. *Remote Sensing of Environment* 95(4): 480-492.

Yasutomi, N.; Hamada, A.; Yatagai, A. 2011. Development of a long-term daily gridded temperature dataset and its application to rain/snow discrimination of daily precipitation. *Global Environmental Research* 15(2): 165-172.

Zargar, A.; Sadiq, R.; Naser, B.; Khan, F.I. 2011. A review of drought indices. *Environmental Reviews* 19(1): 333-349.

IWMI Research Reports

170 *Mapping Multiple Climate-related Hazards in South Asia.* Giriraj Amarnath, Niranga Alahacoon, Vladimir Smakhtin and Pramod Aggarwal. 2017.

169 *Beyond "More Crop per Drop": Evolving Thinking on Agricultural Water Productivity.* Meredith Giordano, Hugh Turral, Susanne M. Scheierling, David O. Tréguer and Peter G. McCornick. 2017.

168 *Global Environmental Flow Information for the Sustainable Development Goals.* Aditya Sood, Vladimir Smakhtin, Nishadi Eriyagama, Karen G. Villholth, Nirosha Liyanage, Yoshihide Wada, Girma Ebrahim and Chris Dickens. 2017.

167 *Reviving the Ganges Water Machine: Potential and Challenges to Meet Increasing Water Demand in the Ganges River Basin.* Upali A. Amarasinghe, Lal Muthuwatta, Vladimir Smakhtin, Lagudu Surinaidu, Rajmohan Natarajan, Pennan Chinnasamy, Krishna Reddy Kakumanu, Sanmugam A. Prathapar, Sharad K. Jain, Narayan C. Ghosh, Surjeet Singh, Anupma Sharma, Sanjay K. Jain, Sudhir Kumar and Manmohan K. Goel. 2016.

166 *Evaluating the Flow Regulating Effects of Ecosystems in the Mekong and Volta River Basins.* Guillaume Lacombe and Matthew McCartney. 2016.

165 *Controlling Floods and Droughts through Underground Storage: From Concept to Pilot Implementation in the Ganges River Basin.* Paul Pavelic, Brindha Karthikeyan, Giriraj Amarnath, Nishadi Eriyagama, Lal Muthuwatta, Vladimir Smakhtin, Prasun K. Gangopadhyay, Ravinder P. S. Malik, Atmaram Mishra, Bharat R. Sharma, Munir A. Hanjra, Ratna V. Reddy, Vinay Kumar Mishra, Chhedi Lal Verma and Laxmi Kant. 2015.

164 *Integrated Assessment of Groundwater Use for Improving Livelihoods in the Dry Zone of Myanmar.* Paul Pavelic, Sonali Senaratna Sellamuttu, Robyn Johnston, Matthew McCartney, Touleelor Sotoukee, Soumya Balasubramanya, Diana Suhardiman, Guillaume Lacombe, Somphasith Douangsavanh, Olivier Joffre, Khin Latt, Aung Kyaw Zan, Kyaw Thein, Aye Myint, Cho Cho and Ye Thaung Htut. 2015.

163 *Demonstrating Complexity with a Role-playing Simulation: Investing in Water in the Indrawati Subbasin, Nepal.* John Janmaat, Suzan Lapp, Ted Wannop, Luna Bharati and Fraser Sugden. 2015.

162 *Landlordism, Tenants and the Groundwater Sector: Lessons from Tarai-Madhesh, Nepal*. Fraser Sugden. 2014.

Electronic copies of IWMI's publications are available for free.
Visit
www.iwmi.org/publications/

Postal Address
P O Box 2075
Colombo
Sri Lanka

Location
127 Sunil Mawatha
Pelawatta
Battaramulla
Sri Lanka

Telephone
+94-11-2880000

Fax
+94-11-2786854

E-mail
iwmi@cgiar.org

Website
www.iwmi.org

IWMI
International Water Management Institute

IWMI is a CGIAR Research Center and leads the:

CGIAR

RESEARCH PROGRAM ON
Water, Land and Ecosystems

ISSN: 1026-0862
ISBN: 978-92-9090-853-1